THE UNIVERSITY OF MICHIGAN
COLLEGE OF ENGINEERING
DEPARTMENT OF ELECTRICAL AND COMPUTER ENGINEERING
Radiation Laboratory

EC-135 SURFACE FIELD MEASUREMENTS ON PERFECTLY CONDUCTING GROUND PLANE: TOP INCIDENCE

By

Valdis V. Liepa

Task Report No. 2, Contract No. F29601-26-C-0004
(1 February 1976 to 31 July 1976)

Prepared for:

Air Force Weapons Center
Kirtland Air Force Base
New Mexico

14182-2-T = RL-2267

Ann Arbor, Michigan
(313) 764-0500

1. INTRODUCTION

This is the second of the series of Task Reports on Contract F29601-76-0004 entitled, "Aircraft Scale Model Measurements and Scaling Verification" and presents the measured surface currents and charges on models of the EC-135 aircraft in the presence of a perfectly conducting ground plane. Topside incidence was always used and, depending on the particular measurement, the incident electric vector was either parallel to the fuselage (symmetric excitation) or perpendicular to the fuselage (anti-symmetric excitation). The measurements were made using 1/375 to 1/114 scale model aircraft by scanning the frequency over the bands 0.45 to 1.1 GHz and 2.0 to 4.0 GHz. The data presented here, however, are for the lower frequency band only, corresponding to the full scale frequencies from 1.38 to 9.65 MHz. The measurements are for models with and without HF wires stretched from the vertical stabilizer of the model to the top of the fuselage near the cockpit.

2. MEASUREMENTS

2.1 Facility and Equipment

The measurements were made in the University of Michigan surface field measurement facility which has been described previously in AFWL-TR-75-217*. For these measurements, a vertical ground plane four feet high and 12 feet wide was erected in the chamber. A framework of 2x4's was used for supporting the 4 x 12 foot 0.030 inch thick aluminum sheet whose side edges were then imbedded into the absorber walls of the chamber to reduce current reflections from the vertical edges. Since the incident field is horizontally polarized, the currents on the sheet are also horizontal.

---

*Liepa, Valdis V., "Sweep Frequency Surface Field Measurements", Univ. of Mich. Rad. Lab. Report No. 013378-1-F, AFWL-TR-75-217, 1975.

The first tests made on the new ground plane were surface scans at a fixed frequency over an area 0.8 by 0.8 m square and there the field amplitude was constant within $\pm$ 0.5 dB. However, when the frequency was scanned with the test sensor at the center of the ground plane, amplitude oscillations on the order of 3 dB appeared on the X-Y recorder trace. This was obviously a source of concern, and after numerous tests and measurements (and arguments on how a matched horn antenna can reradiate a part of the received signal), it was concluded that energy was being reflected by the ground plane back into the horn and then reradiated in- or out-of-phase depending upon the frequency. To reduce this interaction, about 60 percent of the ground plane was covered with an absorber with particular attention paid to feathering the absorber edge near to the center of the plate so as not to introduce adverse current reflections. This reduced the ground plane-horn interaction to about 1.5 dB, and yet a further reduction was obtained by changing the reference signal pickup from a directional coupler located ahead of the transmitter horn to a sensor mounted on the ground plane. This change did not reduce horn-ground plane interaction per se, but did smooth out the recorder trace since both the reference and the test signals increased or decreased simultaneously.

Figure 1 shows the frontal view of the absorber-covered ground plane with a model aircraft mounted at the center. The A/C model is out of proportion—the model shown appears over two feet long, although the largest model used was 1/114 scale and about half the size shown. Figure 2 shows a side view of the same and emphasizes the placement of the reference and test sensors. To accommodate the reference and the (bottom) test sensors, holes 3/8 inches in diameter and spaced 5 cm apart were drilled through the ground plane in an x-y coordinate lattice whose center is at the center of the sheet. The holes spanned 80 cm horizontally and vertically.

By moving the MGL-S8A(R) sensor (the one with connector underneath) through all the mounting positions (holes) and recording the frequency response at each

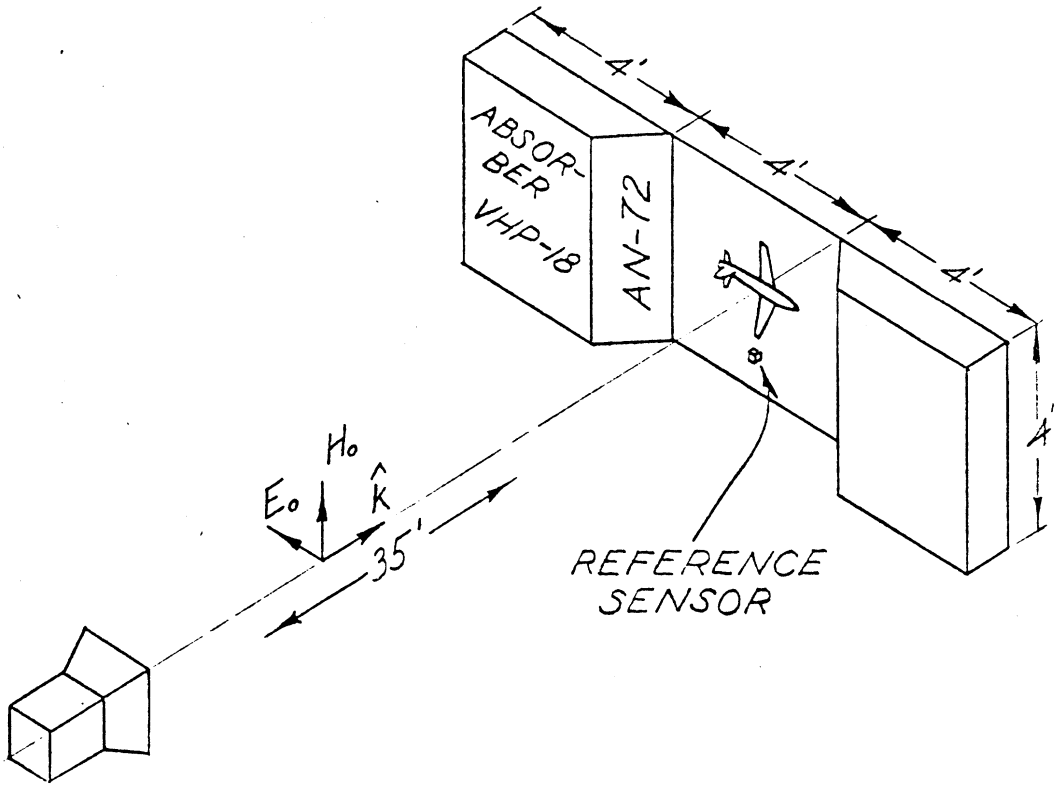

Figure 1. Frontal view of the absorber covered ground plane. The ground plane and the transmitting antenna are inside the anechoic chamber (not shown).

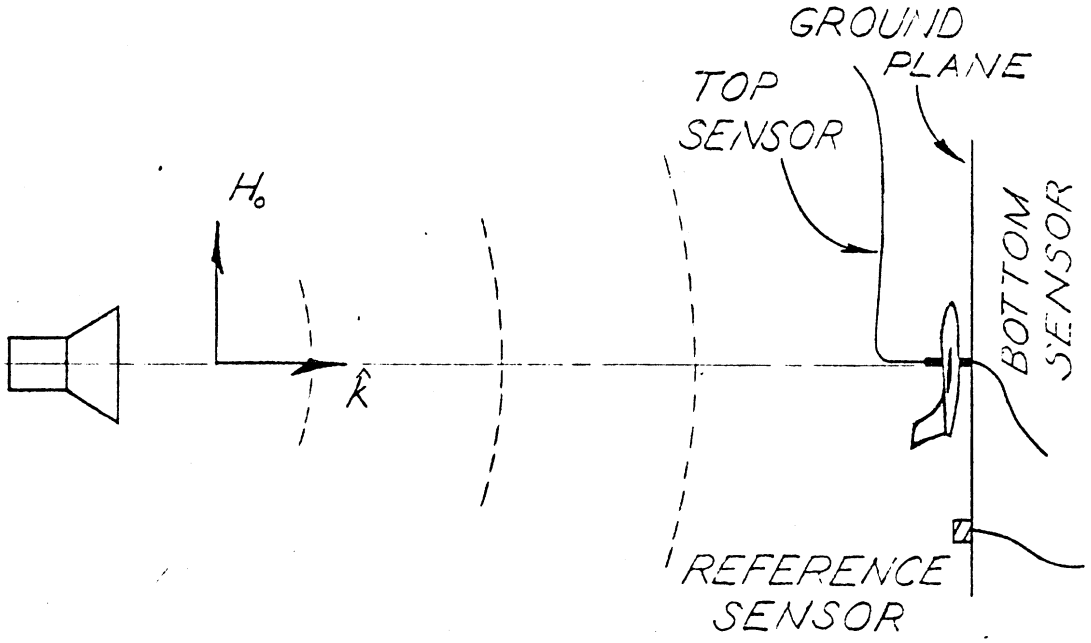

Figure 2. Sideview sketch showing the locations of the sensors (Drawing is not to scale.)

position, vertical and horizontal surface scans were obtained. Figure 3 shows the reduced data for 0.5 and 1.0 GHz. Measurements were also made in the 2 to 4 GHz band and the results there were similar.

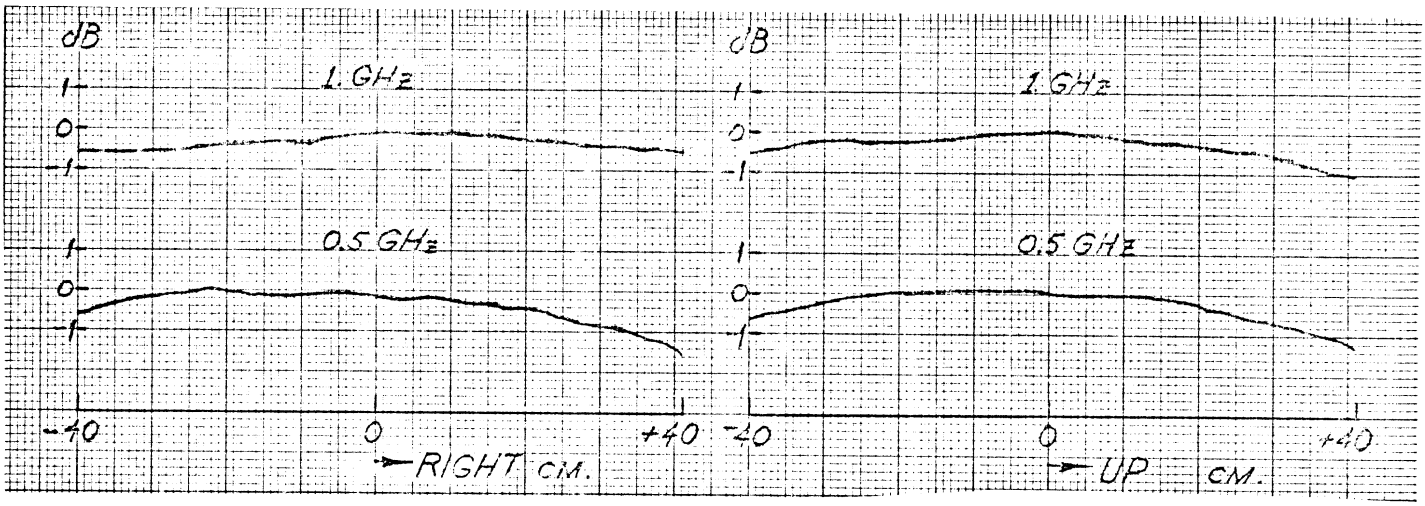

Figure 3. Vertical and Horizontal surface scans made with MGL-S8A(R).

Figure 4 shows the block diagram of the instrumentation used in measurements of the model aircraft near the ground plane. The arrangement is similar to that used earlier in free-space measurements, the main difference being that the reference signal is now taken from a sensor (MGL-S7A(R)) mounted on the ground plane rather than from a directional coupler located ahead of the horn.

2.2 Model

For the measurements, five different models were used ranging in scale from 1/114 to 1/325. These are the same ones previously used for obtaining the free-space data, but because they have been reworked and repainted, some of the scaling factors

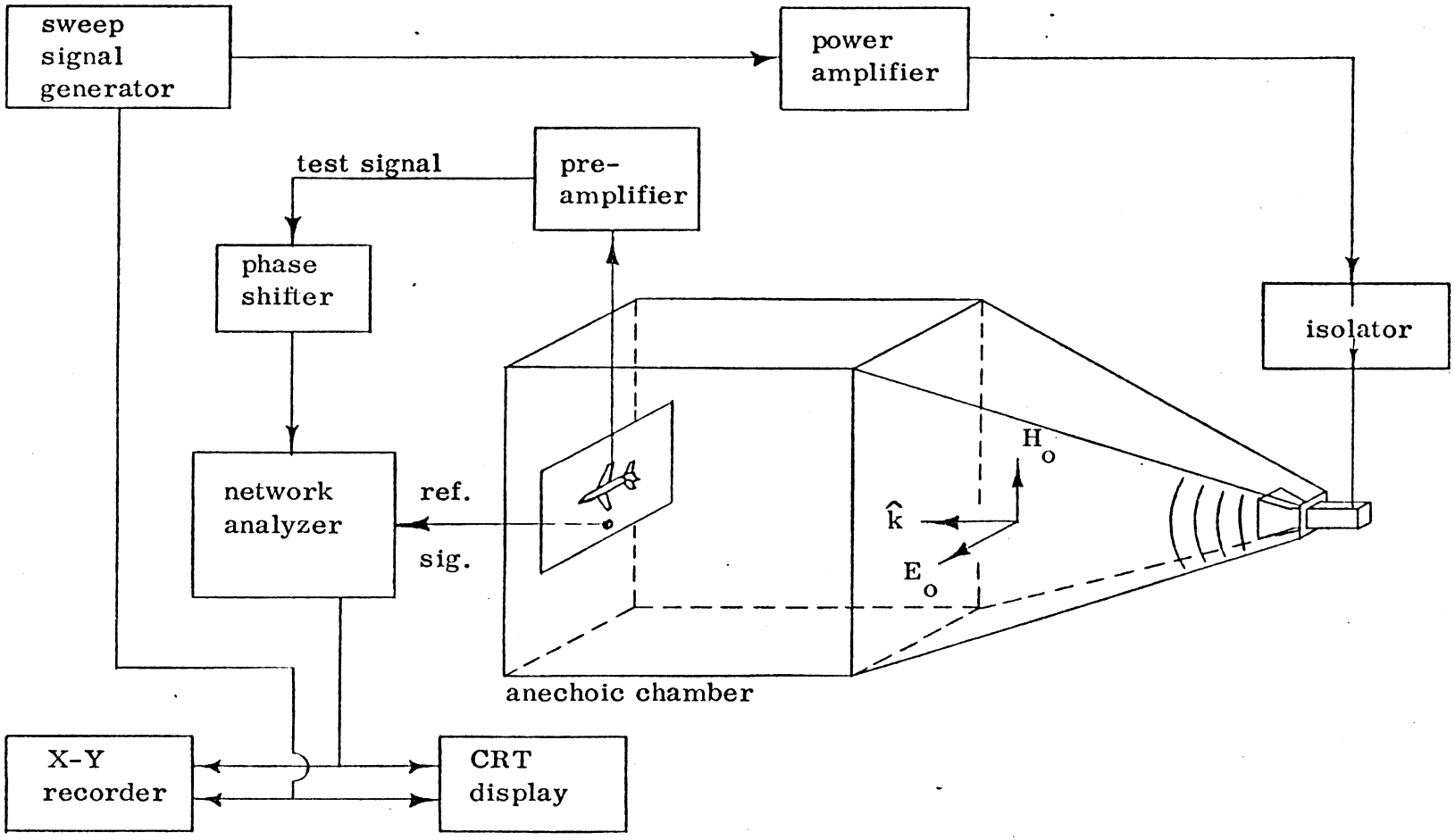

Figure 4. Surface Field Measurement Facility with vertical ground plane.

differ from those originally given. All models are in the "wheels-up" configuration and have wheel wells and doors taped over with adhesive copper tape. There are two 1/325 scale models, one with HF wires and one without. We have only one 1/216 scale model and for this the wires were attached or removed as required. The 1/129 model is without HF wires and the 1/114 model is with them. Figure 5 shows the locations where these wires are attached and also indicate how they are connected, i.e., open circuit or short circuit condition. To raise the models an appropriate distance above the metal ground plane, four styrofoam blocks were used with each model--two under the fuselage and one under each wingtip. The height of these blocks was chosen to simulate 1.22 m fuselage-to-ground clearance on a full-scale EC-135 aircraft.

The vital statistics of models are summarized in Table 1. Amongst other things, the relative nose-to-wing and the wing-to-fuselage center distances are given. Such information is helpful in interpreting the measured data and, in particular, explaining the presence of the second resonance peak near 4 MHz.

2.3 Measurements and Sensors Used

The measurements are for the same aircraft body locations or stations used in the free space measurements, plus additional measurements for the current on the ground plane under the fuselage of the model. The latter measurements are designated by numbers such as F800G, where "G" implies ground plane measurement. Figure 6 shows the locations of the stations and for specifying them the following convention has been adopted: F1200T is the Fuselage station, located on the Top, with 1200 (the number used by the Air Force) indicating the distance in inches from the nose, but with the nose already at 130 instead of 0. Other letters used in station designations are W, B, and G, and refer to Wing, Bottom, and Ground positions respectively. Four different magnetic sensors and one charge probe were used in making these measurements, with

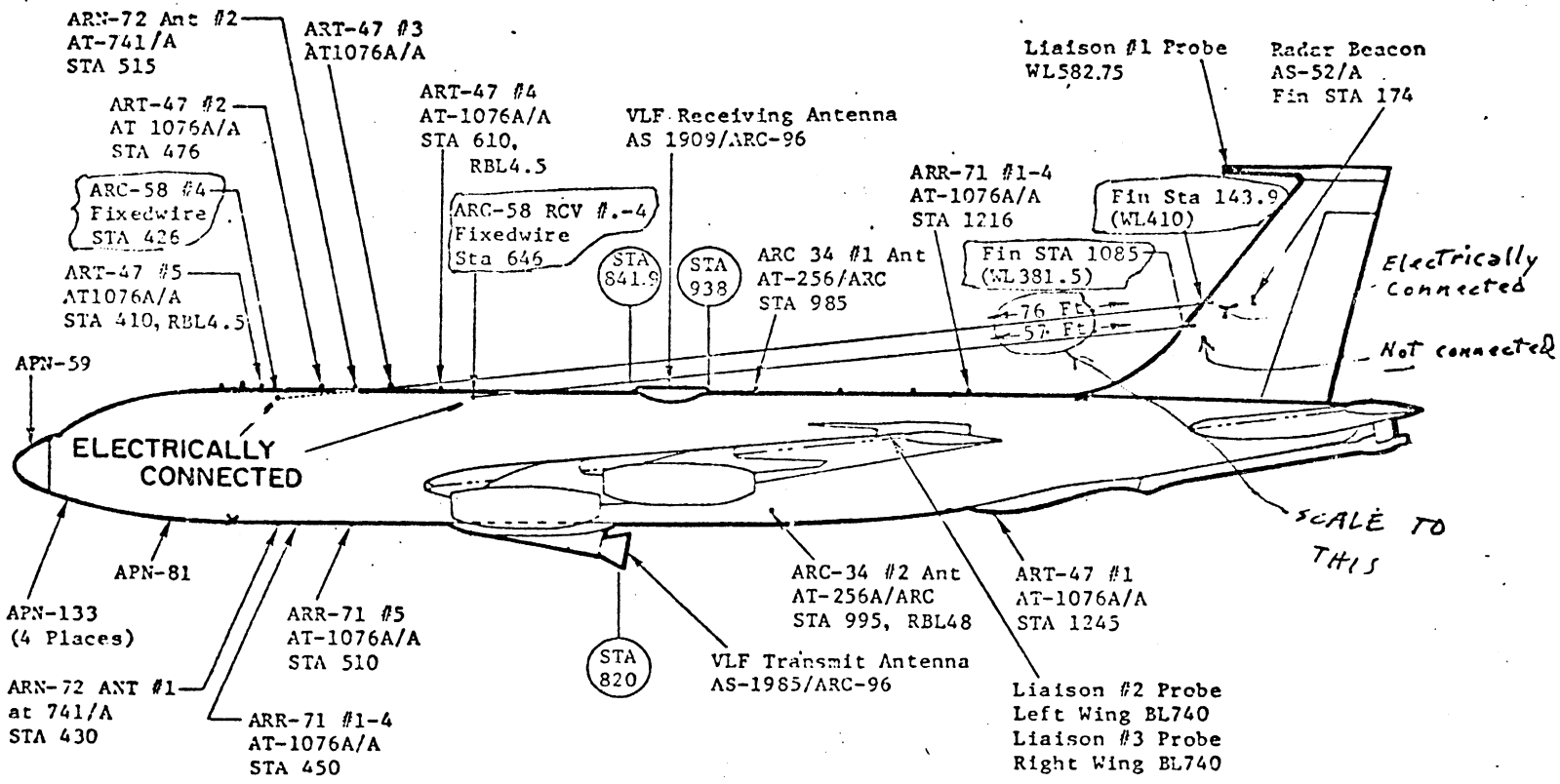

Figure 5. EC-135 HF Wire Antenna Installations

TABLE 1 : EC-135 Models Used

EC-135 Model	Fuselage Scale	Wing Span Scale	Material	Fuselage Height at Station			Wing Thickness at W600	With HF Wires	Without HF Wires	a/L	b/L	$\frac{(a-b)}{L}$
				400 (cm)	800 (cm)	1200 (cm)						
325	1/324.5	1/340.3	metal	1.15	1.19	1.15	0.23	X	X	0.4305	0.5000	0.9305
216	1/216.0	1/225.3	metal	1.80	1.77	1.76	0.28	X		0.3902	0.5307	0.9209
129	1/129.2	1/134.4	plastic	3.01	3.03	3.02	0.59		X	0.3983	0.4807	0.8790
114	1/114.0	1/117.3	plastic	3.50	3.44	3.35	0.30	X		0.3780	0.5621	0.9402

Full Scale Dimensions of EC-135:

Overall length (with boom)	41.53m
Overall length (without boom)	41.17m
Fuselage length (without boom)	39.27m
Wing Span	39.89m
Fuselage clearance	1.22m

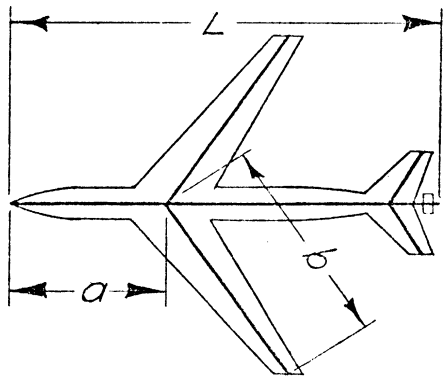

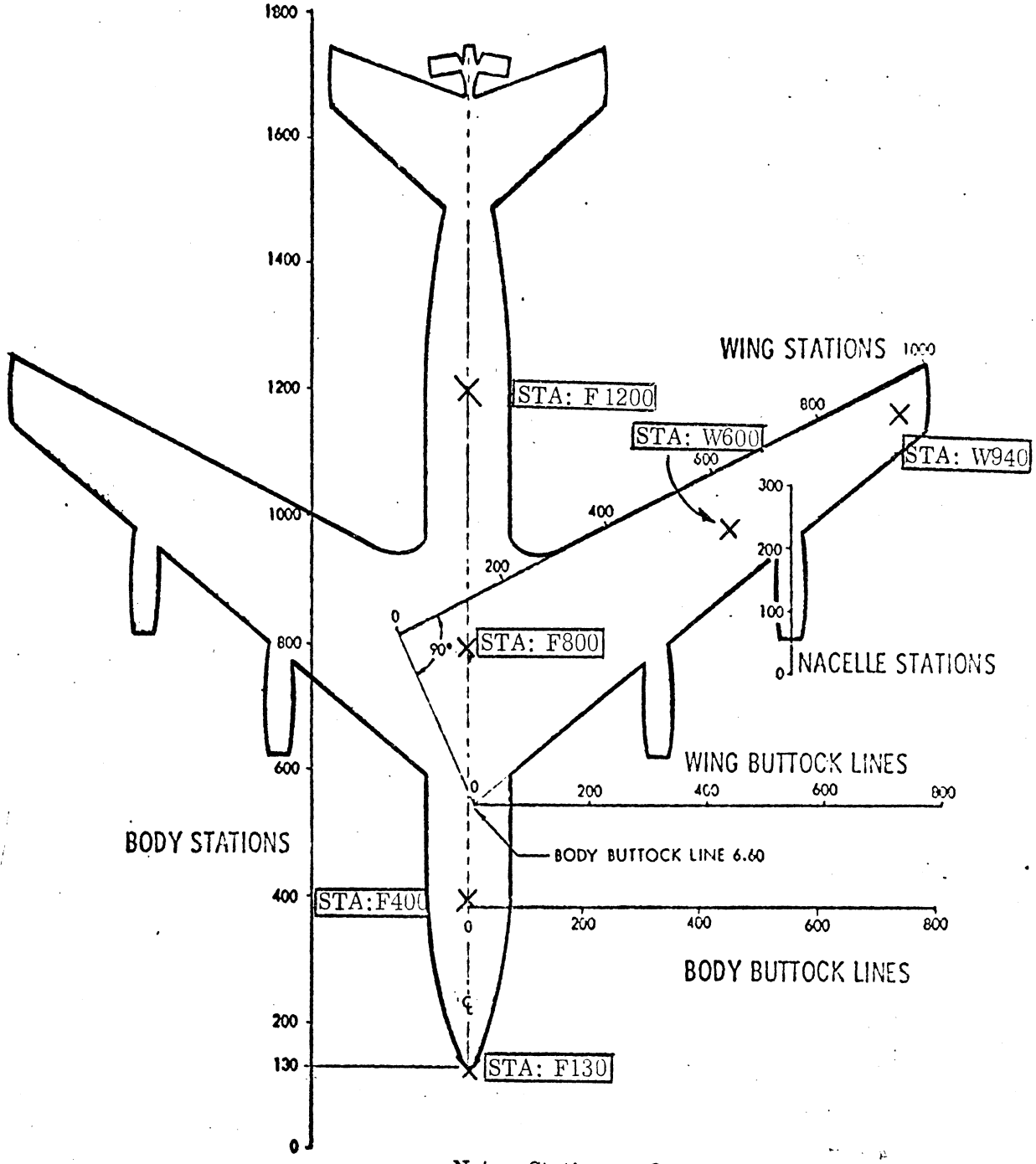

Note: Stations W600 and W940 are at mid-sections of the wing. Station W940 is located at the center of a circle tangent to the three wing edger.

Figure 6. EC-135 Aircraft Body Stations;
X Designates Measurement Locations

the MGL-S7A(A) used for reference. For the top measurements, our own free space 3.2 mm diameter shielded loop probe was used (Figure 2), and for the bottom measurements, a similar but straight probe. The MGL-S8A(R) was used to measure the current on the ground plane, and at the nose and wingtips the charge was measured using a 2 mm extension of the center conductor of a 0.020 inch diameter coax. In all the measurements precautions were taken to minimize the sensor lead interaction with the electromagnetic field.

2.4 Incident Field Calibration

Since it is almost impossible to achieve a flat or even uniform measurement system response over a wide frequency range, the incident field should be measured everytime a sensor or other component in the system is changed. The number of station measurements made per calibration varied. For example, at the F400T, F800T, and F1200T stations, only one calibration run was made for each model and frequency band, while for the bottom stations F400B, F800B, and F1200B, a new calibration run was made for each.

2.4.1 Top Sensor

This is the same one used in the free space model measurements. Its signal lead extends vertically to the ceiling on the illuminated side of the ground plane, but since the lead is perpendicular to the incident electric field, its interaction or disturbance is negligible. For calibration of this sensor and the rest of the system, the loop was moved against the ground plane (with the model removed) and the calibration field $\underline{H}_c$ recorded on the X-Y chart recorder. Hence, the incident field $\underline{H}_o$ is

$$\underline{H}_o = 1/2\, \underline{H}_c \qquad (1)$$

2.4.2 Bottom Sensor

As can be seen in Figure 2, this sensor goes through a small hole in the ground plane. Behind the ground plane the sensor is attached to a precision slide which provides accurate positioning. In measurements of the current at STA:F800B, for example, the model is first mounted on the ground plane and then the sensor is moved out until the loop barely touches the model at this station. To record the calibration field, the model is removed and the field recorded. If h is the distance (or clearance) from the ground plane to what was STA:F800B, the incident field can be written as

$$\underline{H}_o = \frac{\underline{H}_c}{2\cos(kh)}$$

where k is the wave number, i.e.,

$$\underline{H}_o = \frac{\underline{H}_c}{2\cos(12fh)} \qquad (2)$$

where f is now the frequency in GHz and h is the distance in centimeters.

2.4.3 Wing Measurement

The wing measurement data are for anti-symmetric excitation only, for which the incident magnetic vector is parallel to the fuselage. To measure the wing current, the top and bottom loops were both rotated 34 degrees, the estimated average swept-back angle for the wings. The incident field is then given by

$$\underline{H}_o = \frac{\underline{H}_c}{2\cos 34^o \cos(kh)}, \quad \text{i.e.}$$

$$\underline{H}_o = \frac{\underline{H}_c}{1.6581\cos(12fh)} \qquad (3)$$

where f is the frequency in GHz and h is the displacement of the sensor from the ground plane when the calibration measurement is made. For the wing top measurements, the sensor was always moved against the ground plane and hence h = 0. For the wing bottom measurement, the sensor was left at the wing station location (with the model removed) and hence h is the ground to station distance for the particular model used.

2.4.4 Charge Sensors

Since the 2 mm extensions of the center conductor of the 0.020 inch coax require a base or image plane, a 10 by 10 cm image plane was used to obtain the calibration field. Figure 7 shows its implementation. An L-shaped bracket, made out of 0.020 inch thick brass, was taped to the ground plane perpendicular to the incident electric vector. A coax with center conductor extended was then inserted through the holes previously drilled and carefully taped with conductive tape to cover the loop created on the underside of the image plane. A loop as seen in Figure 7 will respond to the magnetic field, and if not properly hidden, would affect the electric field measurements.

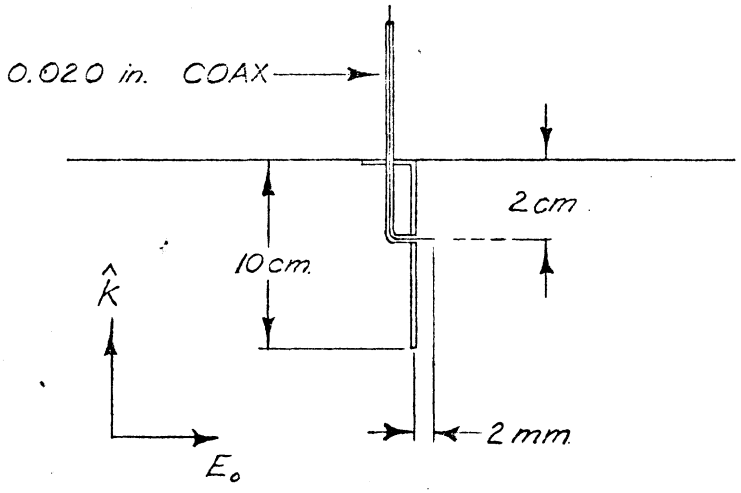

Figure 7. Image plane for calibration of charge probes.

To verify that the field measured on this small image plane is the same as that measured on a larger sheet, we ran frequency scans as the size of the image plane was increased in four increments to 25 by 25 cm square. When compared to the trace for the 10 by 10 cm plane, the recordings typically deviated $\pm$ 0.25 dB over the 0.45 to 1.10 GHz range scanned, and the maximum deviation observed was 0.5 dB. Such variations are within the measurement repeatability tolerances and hence a 10 by 10 cm plate is of sufficient size for the present application.

When a plane wave of strength $\underline{E}_o$ and $e^{i\omega t}$ time dependence is incident perpendicularly on a perfectly conducting ground plane, the sum of the incident and reflected fields is

$$\underline{E} = 2i\underline{E}_o \sin(kd)$$

where d is the distance from the ground plane where $\underline{E}$ is observed. The factor "i" in the equation implies a 90 degree phase shift. If $\underline{E}_c$ represents the calibration voltage measured on the image plane, the incident field $\underline{E}_o$ is then

$$\underline{E}_o = \frac{\underline{E}_c}{2i \sin(kd)}, \quad \text{i.e.,}$$

$$\underline{E}_o = \frac{\underline{E}_c}{2i \sin(12fd)} \tag{4}$$

The charge measurements on the models were made at two stations: the nose (F130, symmetric excitation) and the wingtip (W940T, anti-symmetric excitation). For both measurements, the coax lead was brought away from the model at station F870B and then directly through a hole in the ground plane. The station F870B was selected as a result of the following test. A model was mounted on the ground plane as if for

measuring the current at STA:1200T, but this time a shorting strap to simulate the lead that is present in charge measurements was connected from the bottom of the fuselage to the ground plane. Measurements were then made as the position of the shorting strap was changed, and of the points tested, the STA:F870B was found to have least effect on the current on the top of the fuselage. In the case of anti-symmetric excitations, the charge is zero at any symmetric point on the fuselage, and hence STA:870B was particularly convenient.

2.5 Reduction of Data

The data presented here were manually reduced by picking discrete frequency values, writing down the dB and phase data in a table, and performing the necessary mathematical operations using a hand calculator. Uniformly spaced points were usually chosen along the frequency scale, plus extra points at peaks and other places where the reduced curves were inadequate. The actual points where the data were reduced are shown on the curves.

A correction for the integrating effect of a probe was applied only to the measured data for the charge at the nose (STA: F130). It was assumed that the nose can be approximated as the tip of a prolate spheroid, and using the static solution and the assumption that the 2 mm long monopole responds to the electric field value at its center, i.e., 1 mm from the surface, the following correction factors γ were obtained and applied to the data:

Scale	γ
1/114	1.621
1/129	1.701
1/216	2.174
1/325	2.755

In contrast to the free space data previously given for the current, no corrections to account for the integrating effect of the probe have been applied to the present data. The reason is that with a ground plane present, the illuminating signal can be considered as two plane waves traveling in opposite directions, and for this case we have not yet developed an appropriate correction procedure. Judging from the free space correction data, the correction factor would be at most 1.2 for the 1/325 model and at most 1.15 for the 1/114 model. This factor would apply to the scattered component of the field only, and is therefore applicable to the curves presented only when $H^{scat} \gg H_o$, i.e. $H/H_o \gtrsim 10$.

3.0 DATA

The surface current and charge data presented has been normalized to the incident field strength H_0 or E_0 and scaled to the full scale frequencies. Figures designated XXa contain amplitude data, and those designated XXb contain the corresponding phase data. Note that the phase is relative to the incident phase at the ground plane surface. Also, the first pair of figures for a given station is for the model without HF wires, followed by the data for the model with wires. Table 2 summarizes the data and can be used as a guide to quickly locate a particular set.

All the measurements that were made under this task are included. Most of the results appear excellent and quite consistent, yet there are some "rotten apples" indicating that something abnormal may have happened when the data was taken. Because the reduction of the data lags the measurements by a month or so, it is impractical to repeat the measurements in question. Where abnormalities in data occur and there is an apparent reason for the effects, comments have been entered on the figures. The data reduction for some of the measurements is being rechecked and if any gross errors are found, corrections will be forwarded to the Air Force.

Table 2. Data Selection Chart

Station Number	J or Q	Without HF wires		With HF wires	
		Symmetric (Figure)	Anti-Symmetric (Figure)	Symmetric (Figure)	Anti-Symmetric (Figure)
F400T	J	8a, b	-----	9a	-----
F800T	J	10a, b	20a, b	11a	21a
F1200T	J	12a, b	-----	13a	-----
F400B	J	14a, b	-----	15 a	-----
F800B	J	16a, b	22a, b	17a	23a
F1200B	J	18a, b	-----	19a	-----
W600T	J	-----	24a, b	-----	25a
W600B	J	-----	26a, b	-----	27a
F130	Q	28a, b	-----	29a	-----
W940T	Q	-----	30a, b	-----	31a
F400G	J	-----	-----	-----	-----
F800G	J	32a, b	34a, b	-----	-----
F1200G	J	33a, b	35a, b	-----	-----

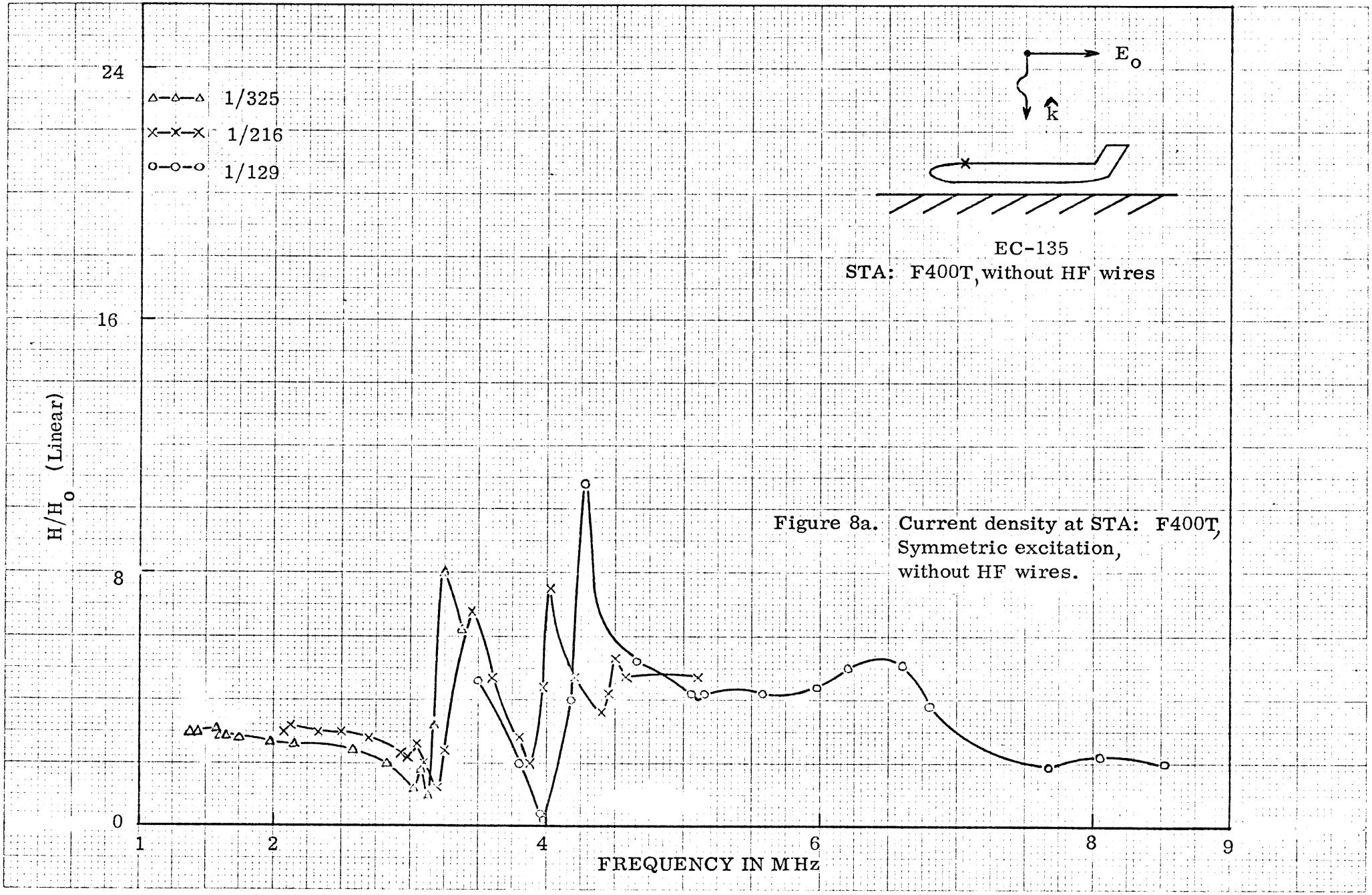

Figure 8a. Current density at STA: F400T, Symmetric excitation, without HF wires.

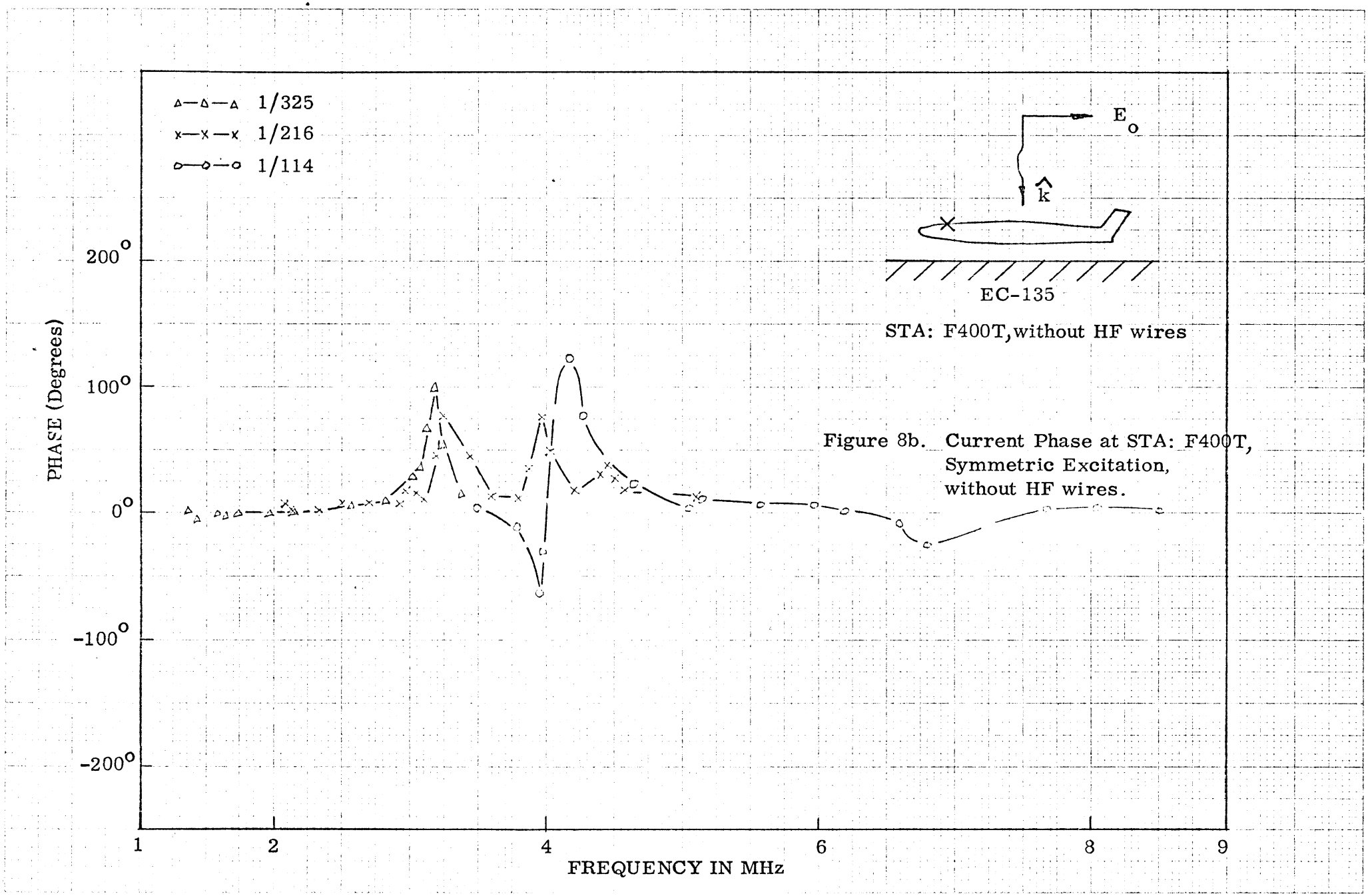

Figure 8b. Current Phase at STA: F400T, Symmetric Excitation, without HF wires.

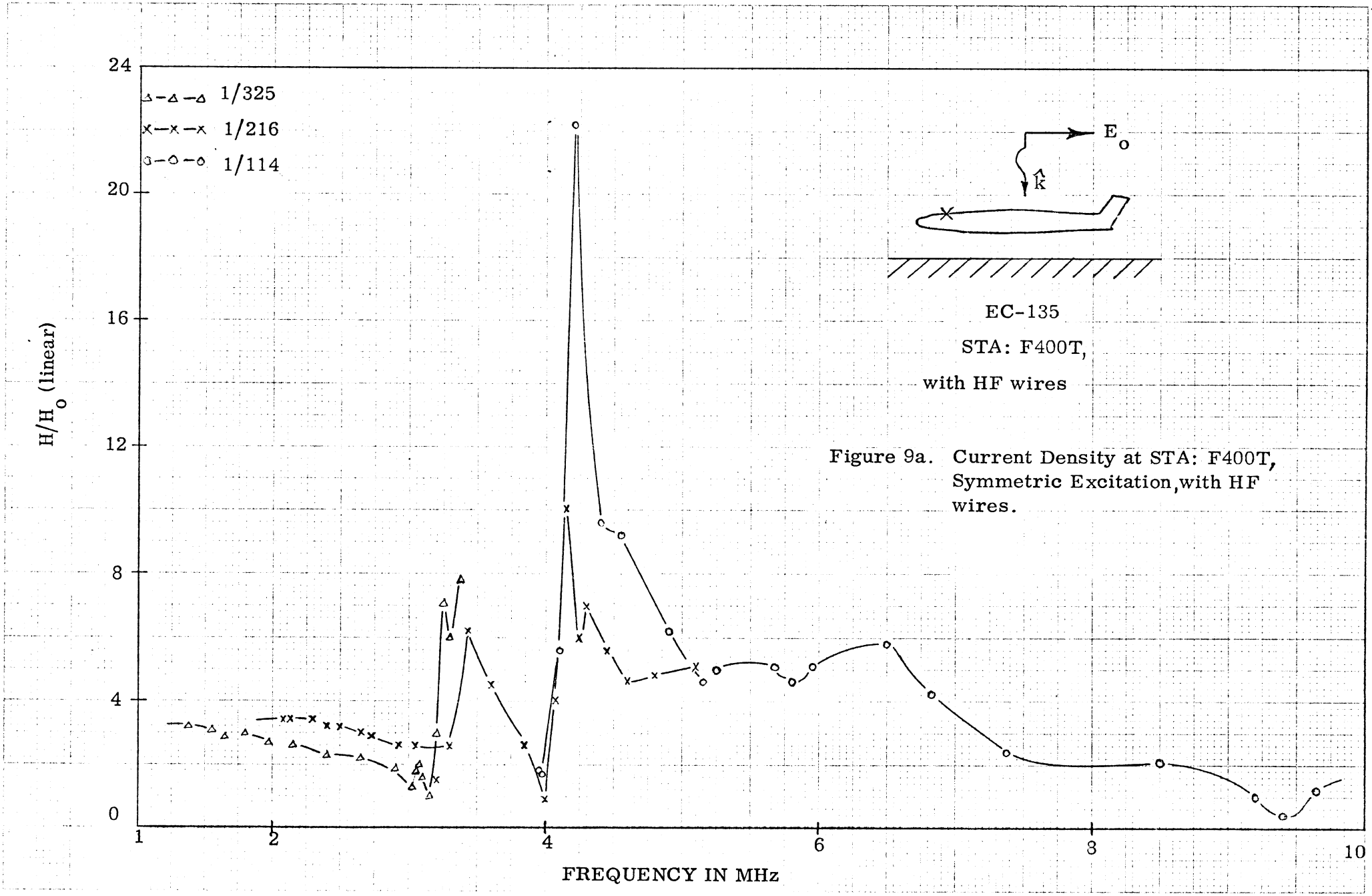

Figure 9a. Current Density at STA: F400T, Symmetric Excitation, with HF wires.

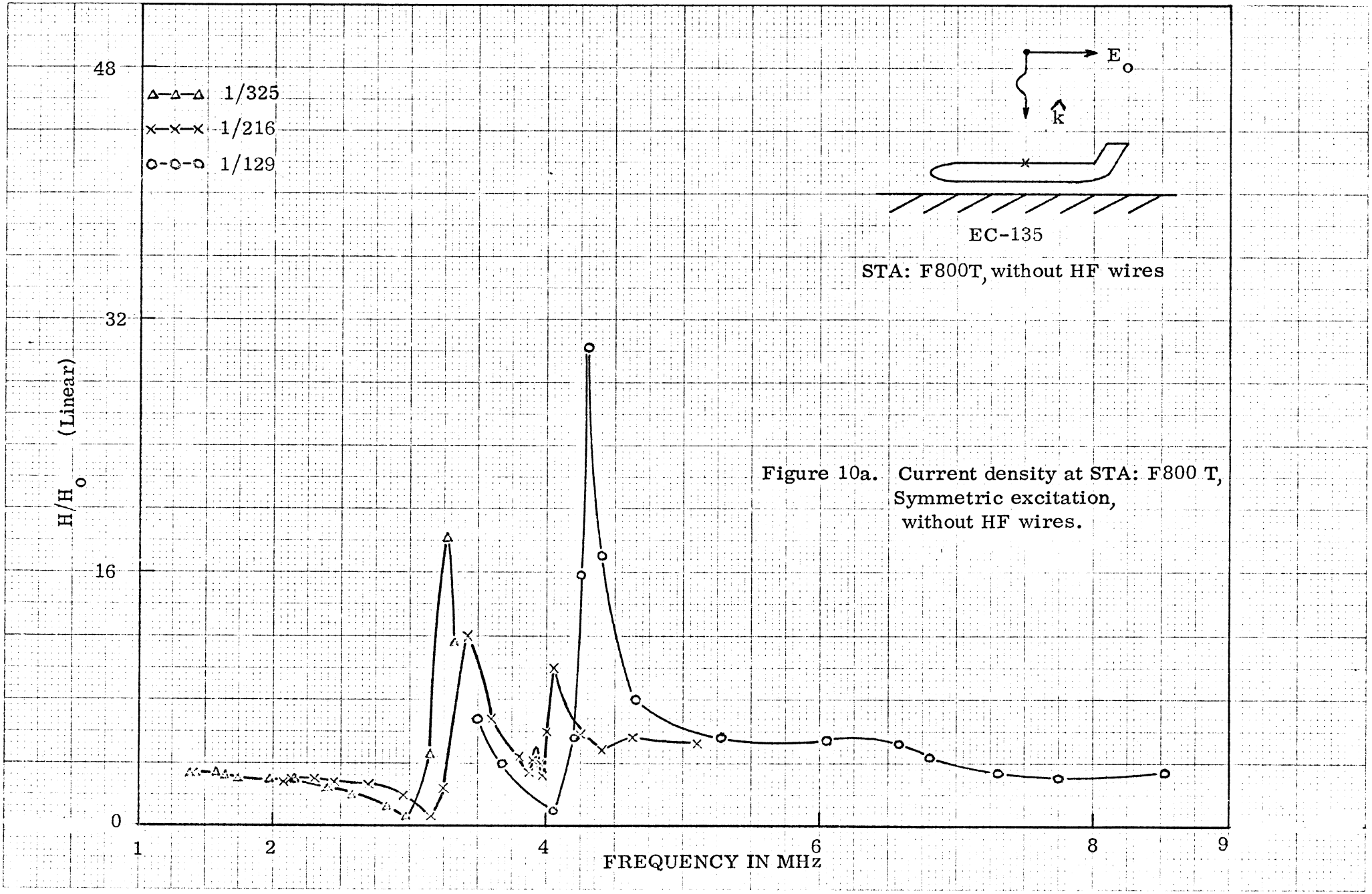

Figure 10a. Current density at STA: F800 T, Symmetric excitation, without HF wires.

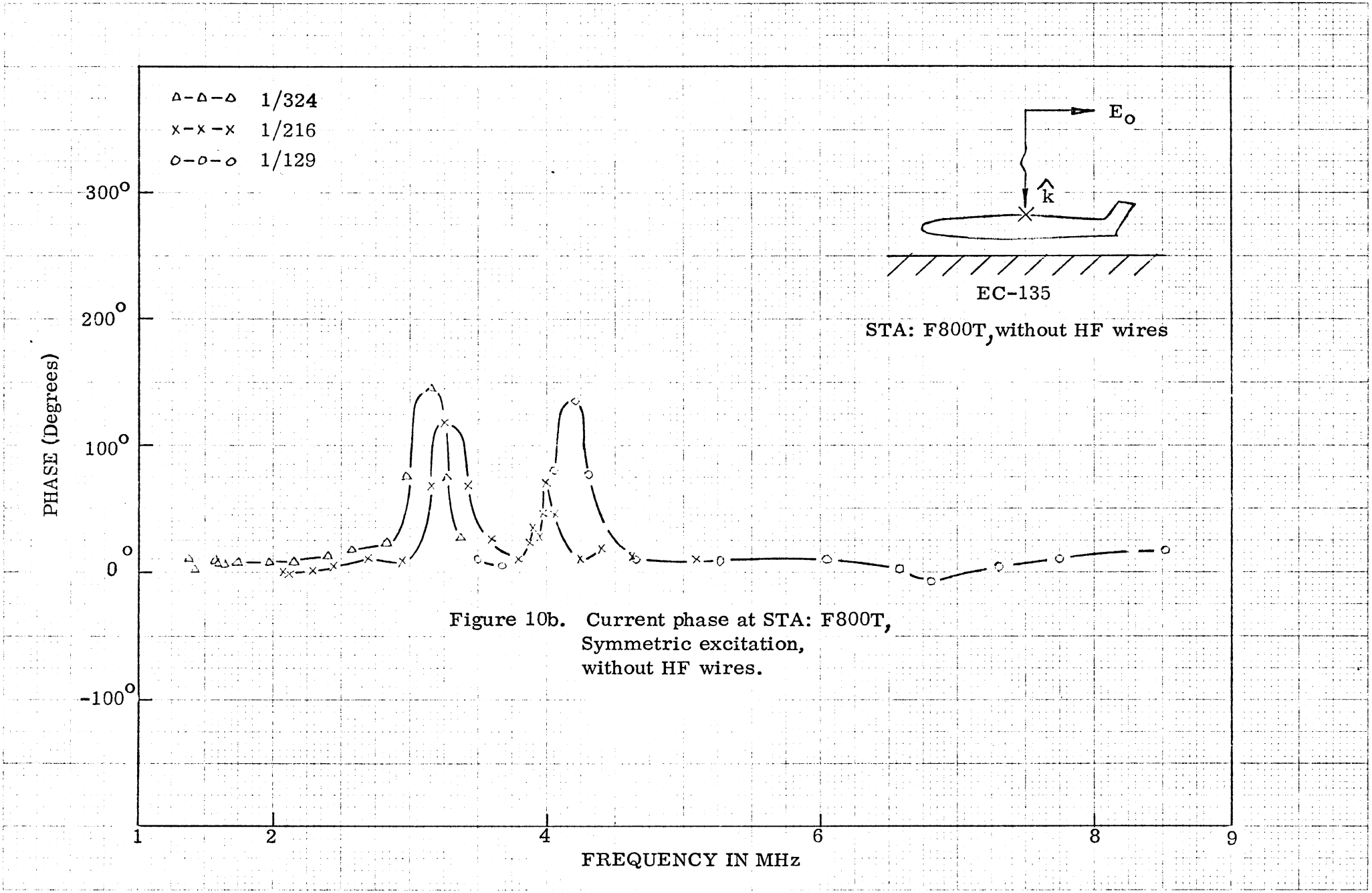

Figure 10b. Current phase at STA: F800T, Symmetric excitation, without HF wires.

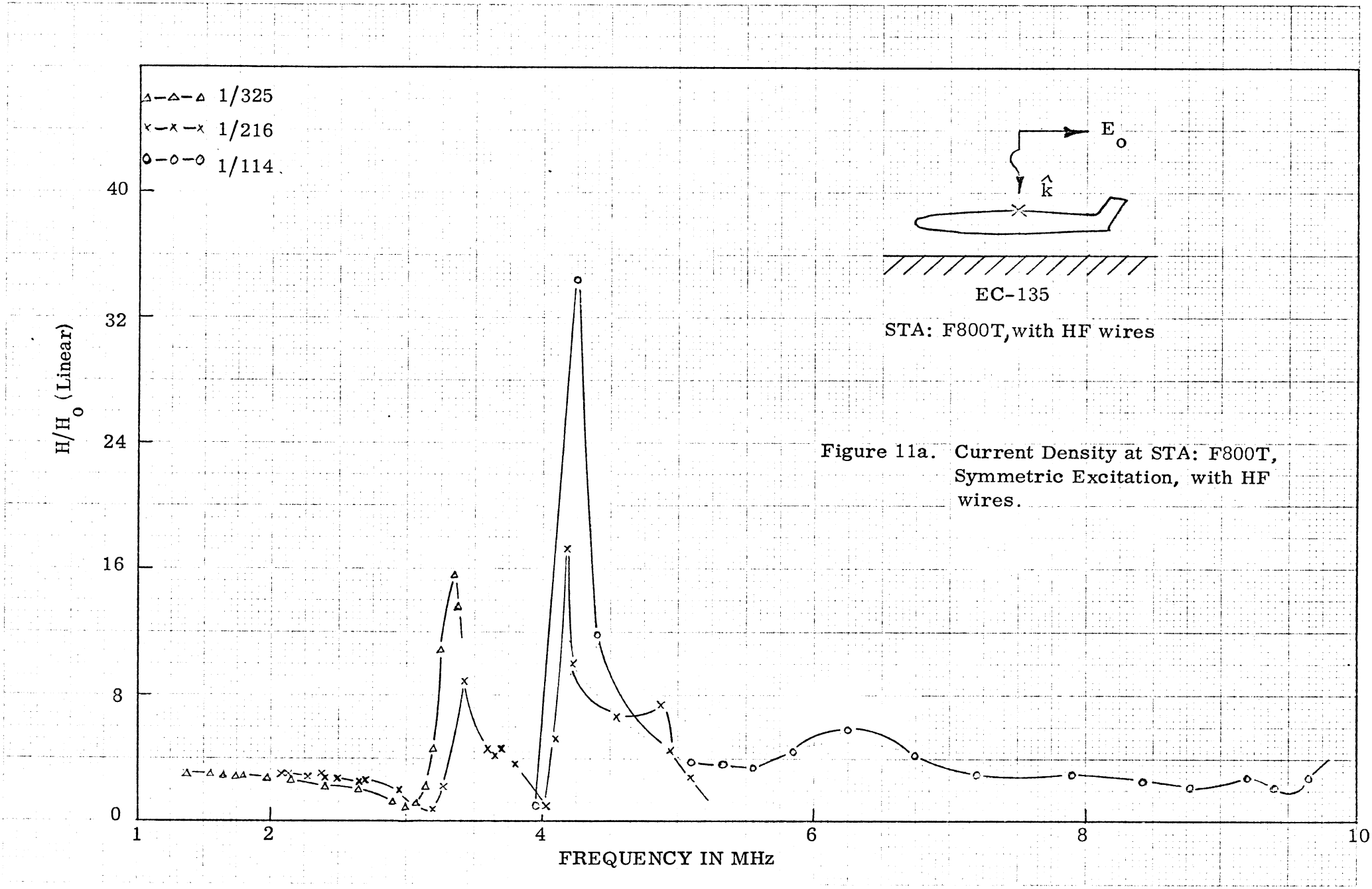

Figure 11a. Current Density at STA: F800T, Symmetric Excitation, with HF wires.

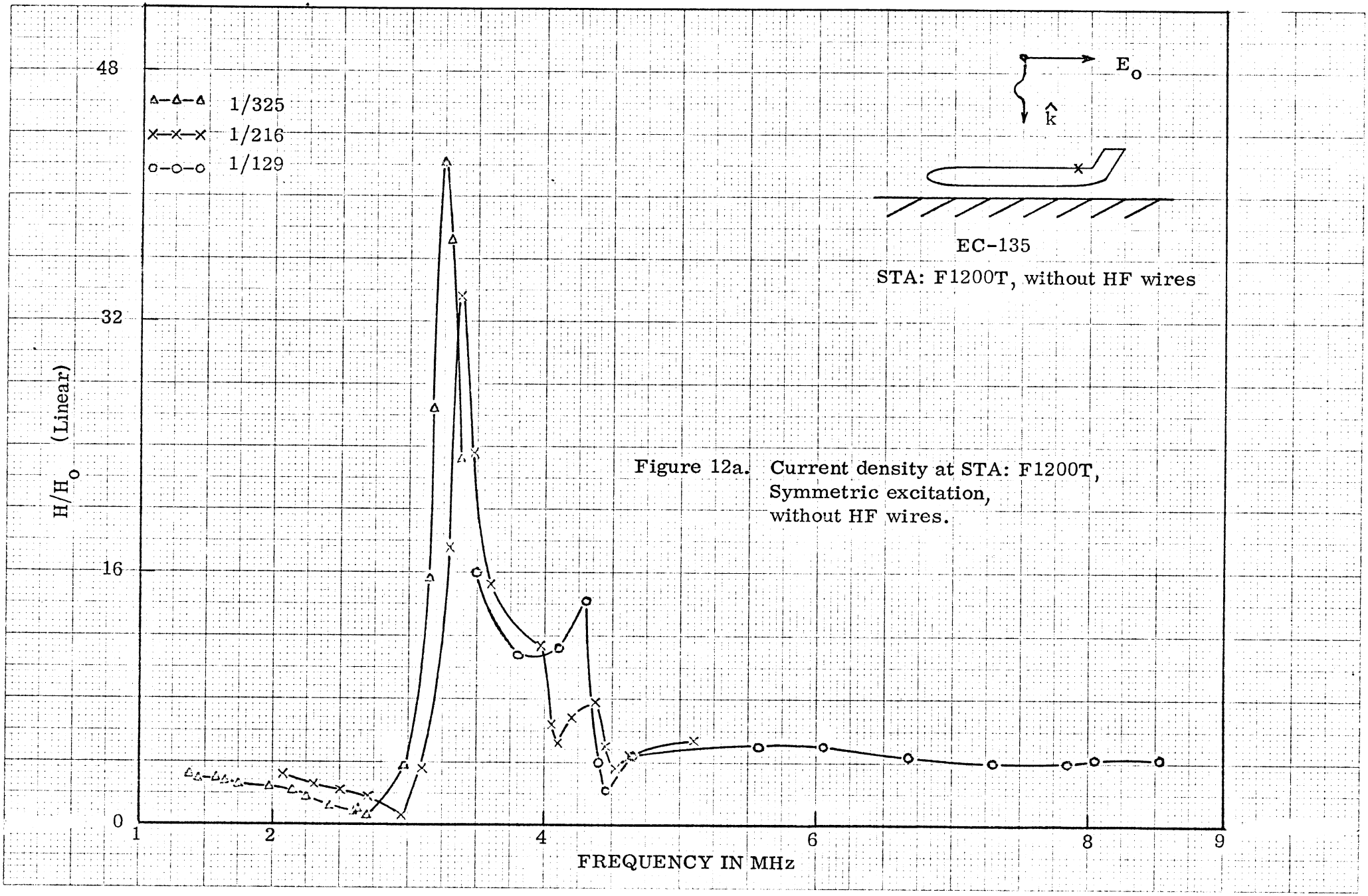

Figure 12a. Current density at STA: F1200T, Symmetric excitation, without HF wires.

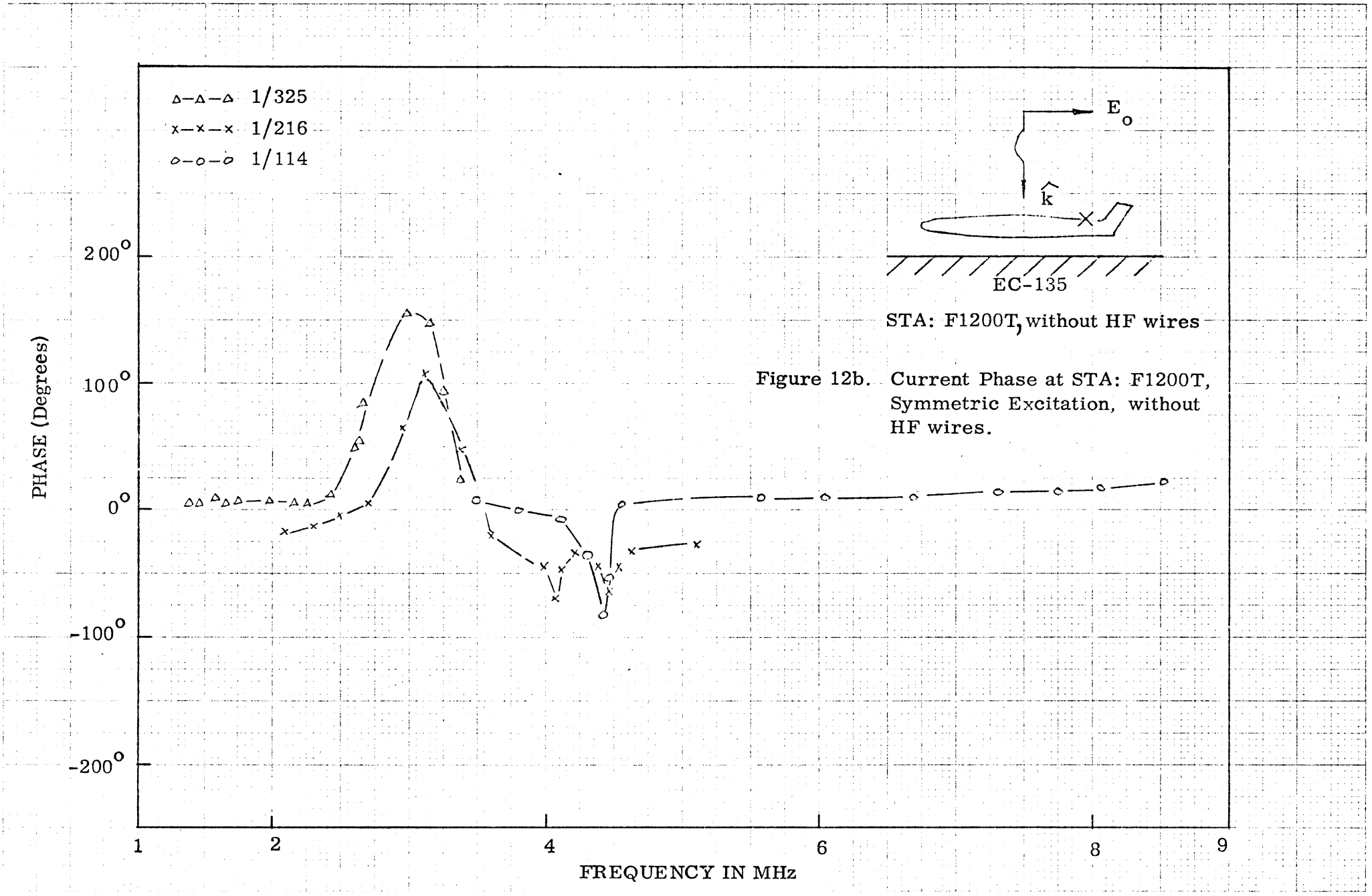

Figure 12b. Current Phase at STA: F1200T, Symmetric Excitation, without HF wires.

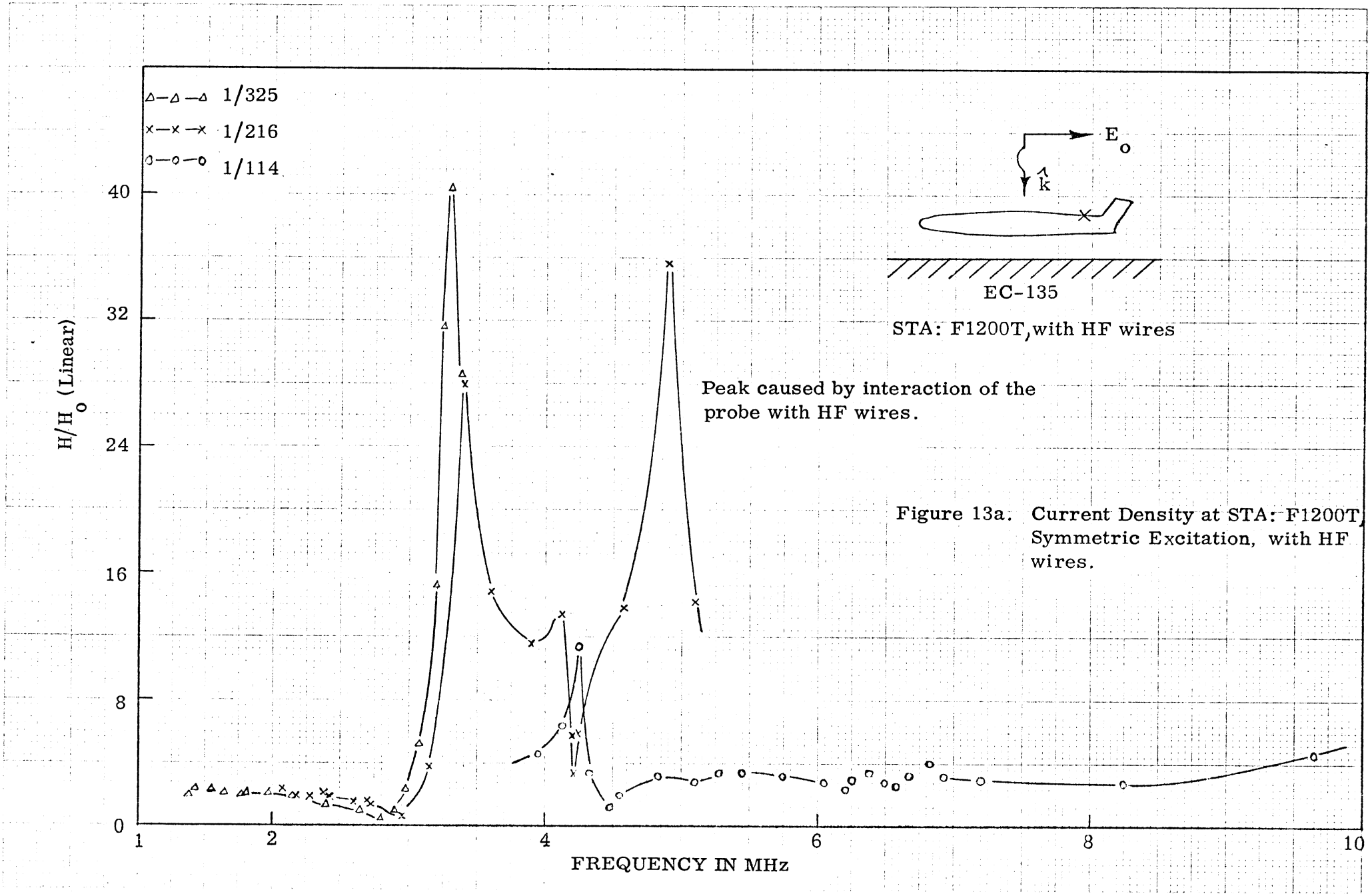

Figure 13a. Current Density at STA: F1200T, Symmetric Excitation, with HF wires.

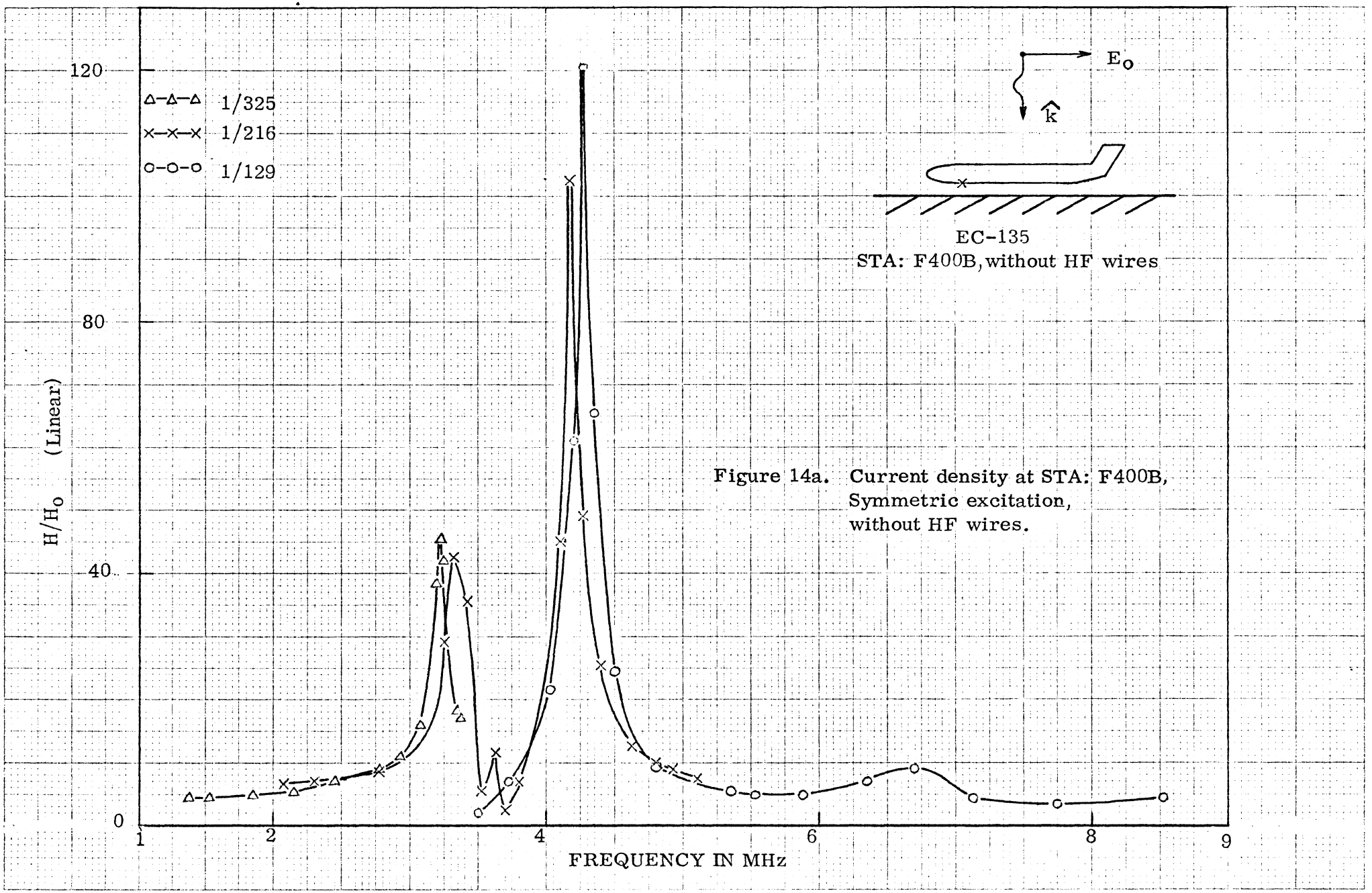

Figure 14a. Current density at STA: F400B, Symmetric excitation, without HF wires.

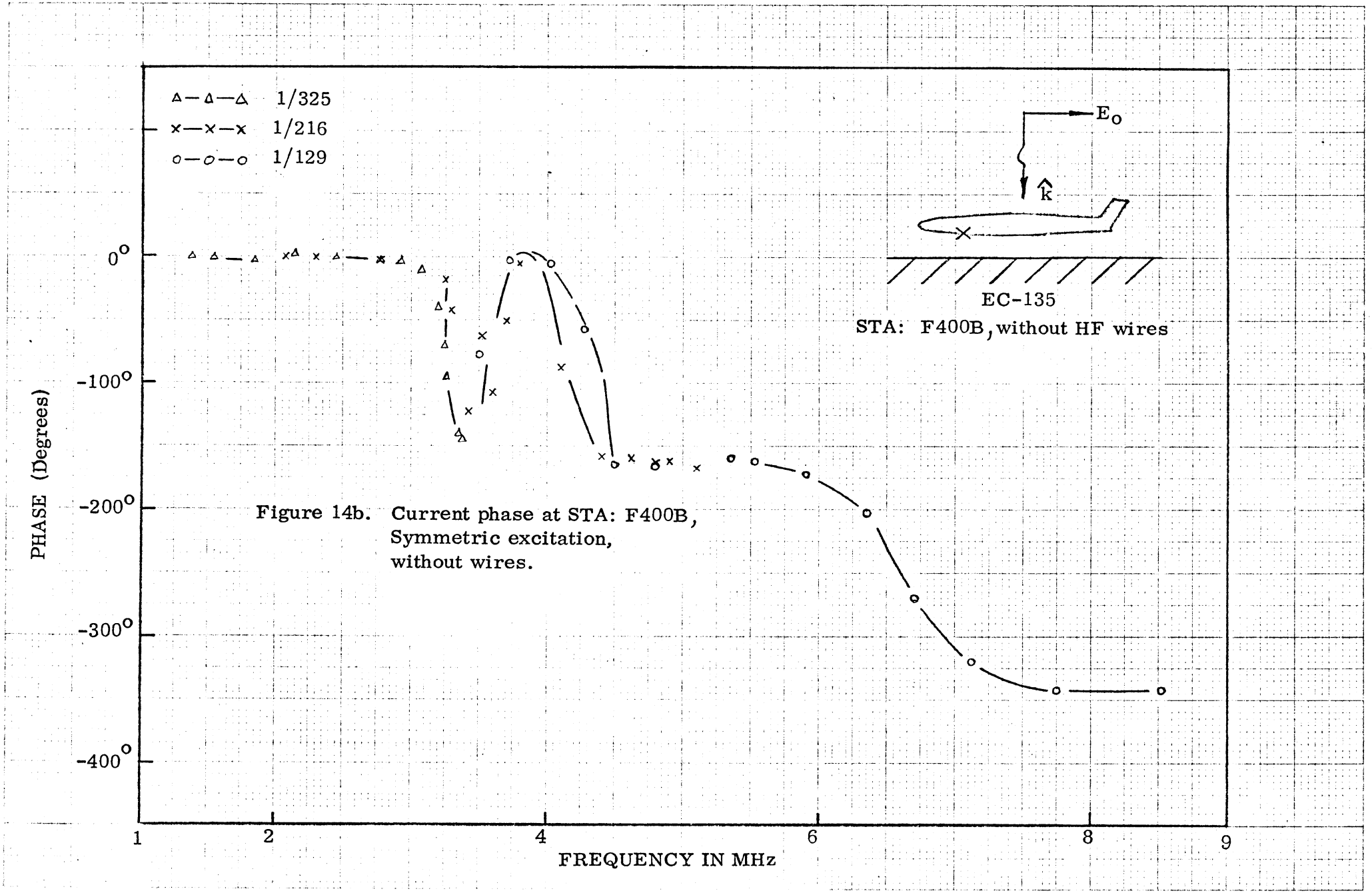

Figure 14b. Current phase at STA: F400B, Symmetric excitation, without wires.

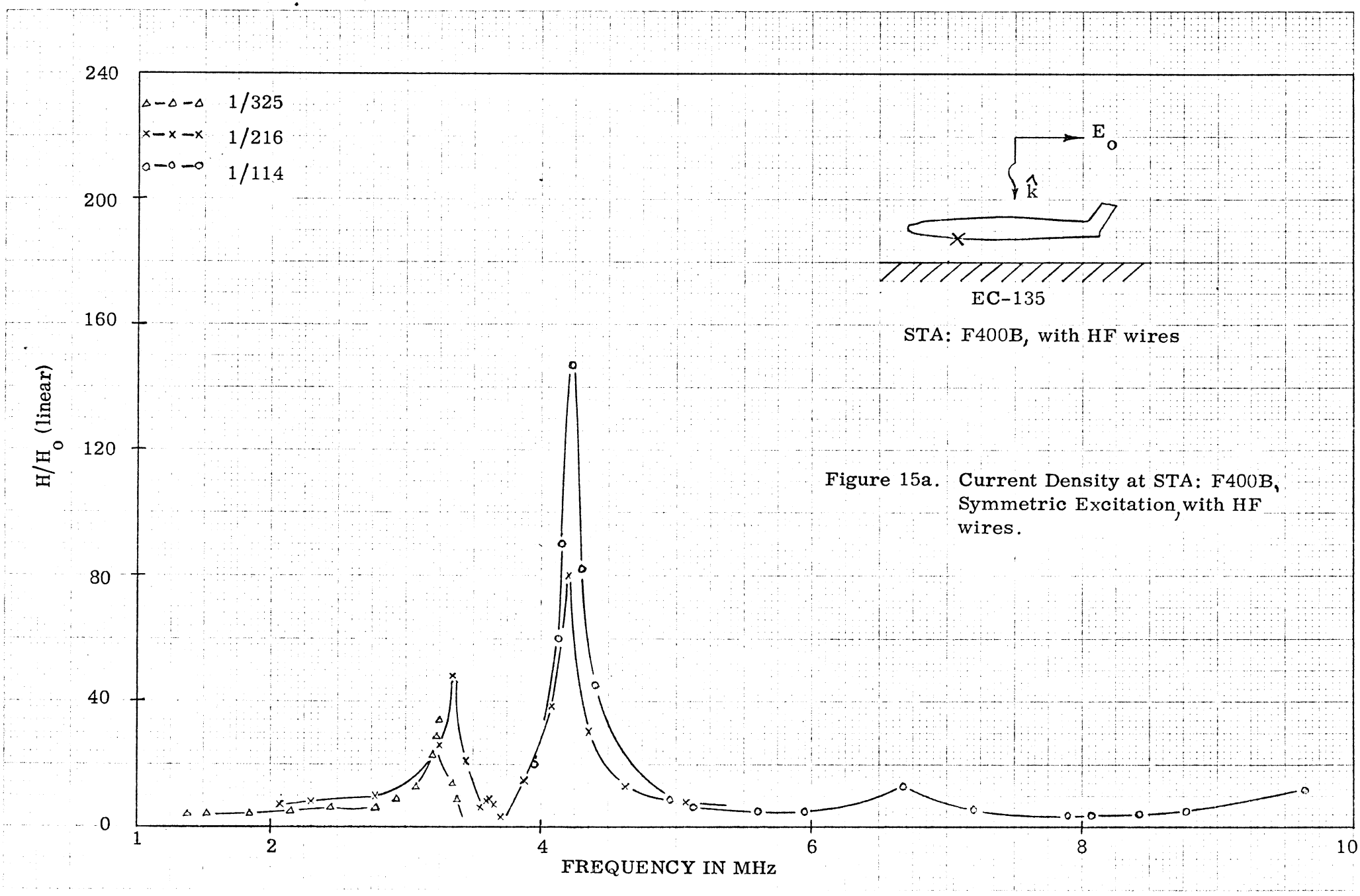

Figure 15a. Current Density at STA: F400B, Symmetric Excitation, with HF wires.

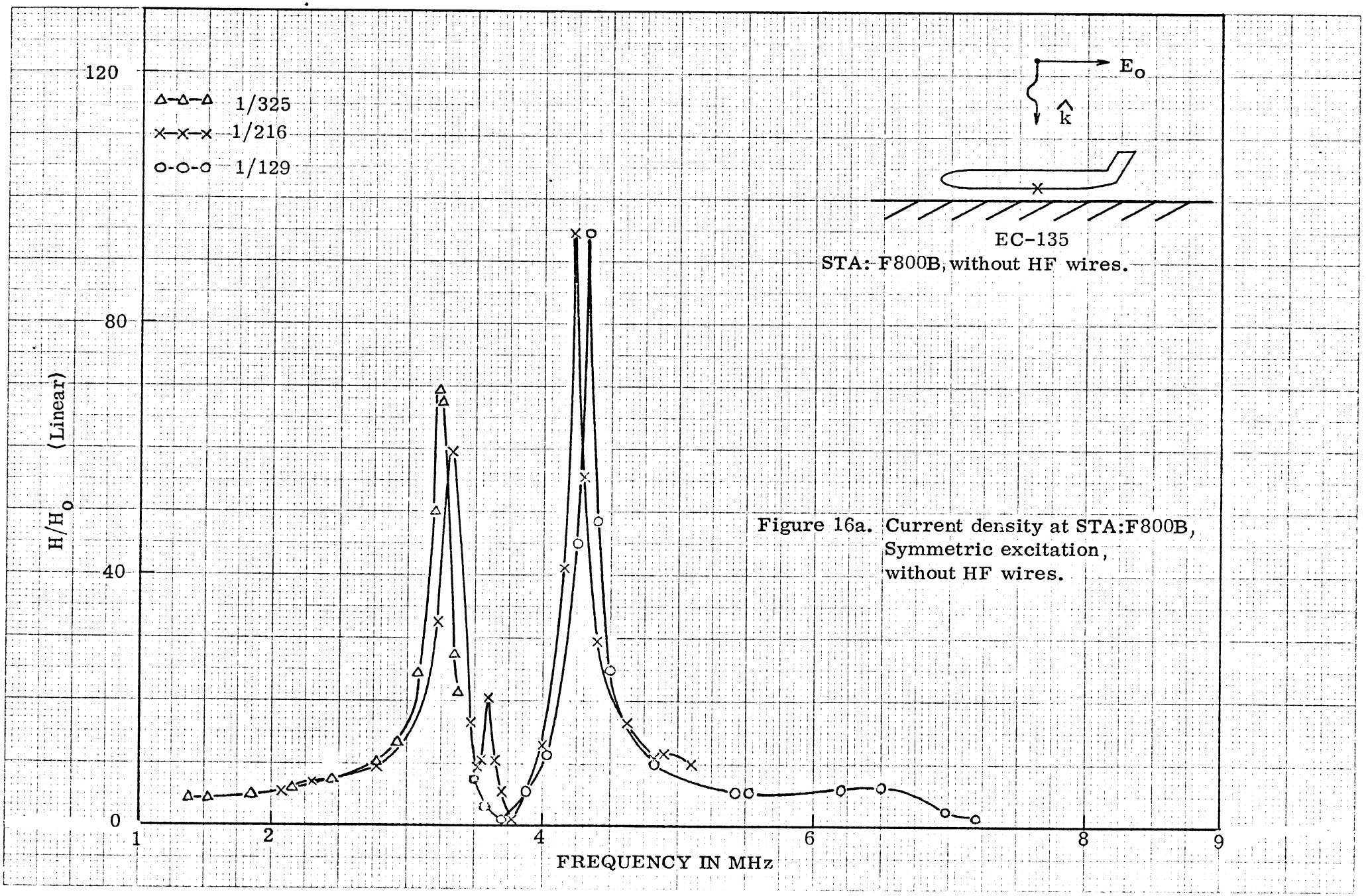

Figure 16a. Current density at STA:F800B, Symmetric excitation, without HF wires.

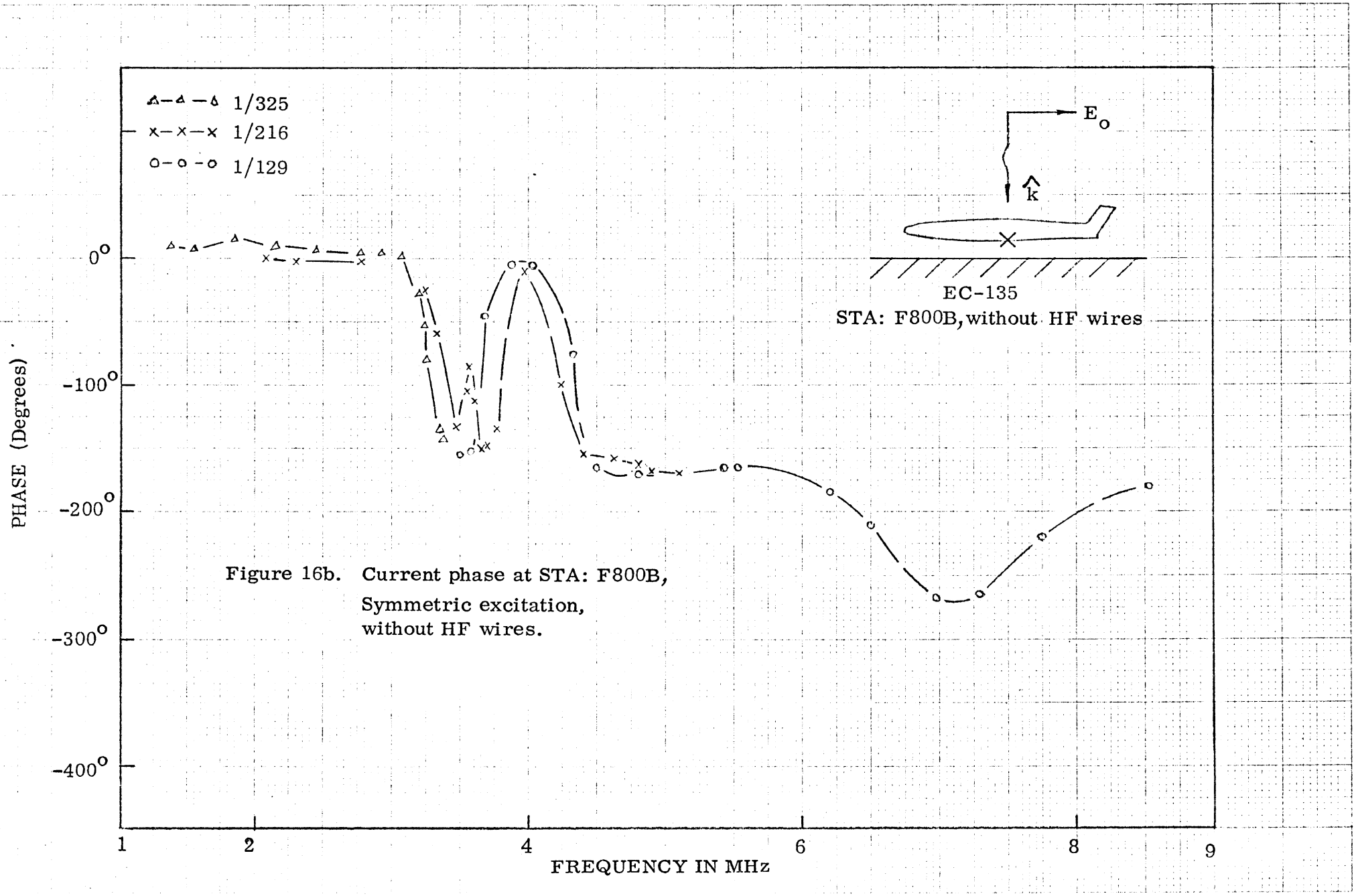

Figure 16b. Current phase at STA: F800B, Symmetric excitation, without HF wires.

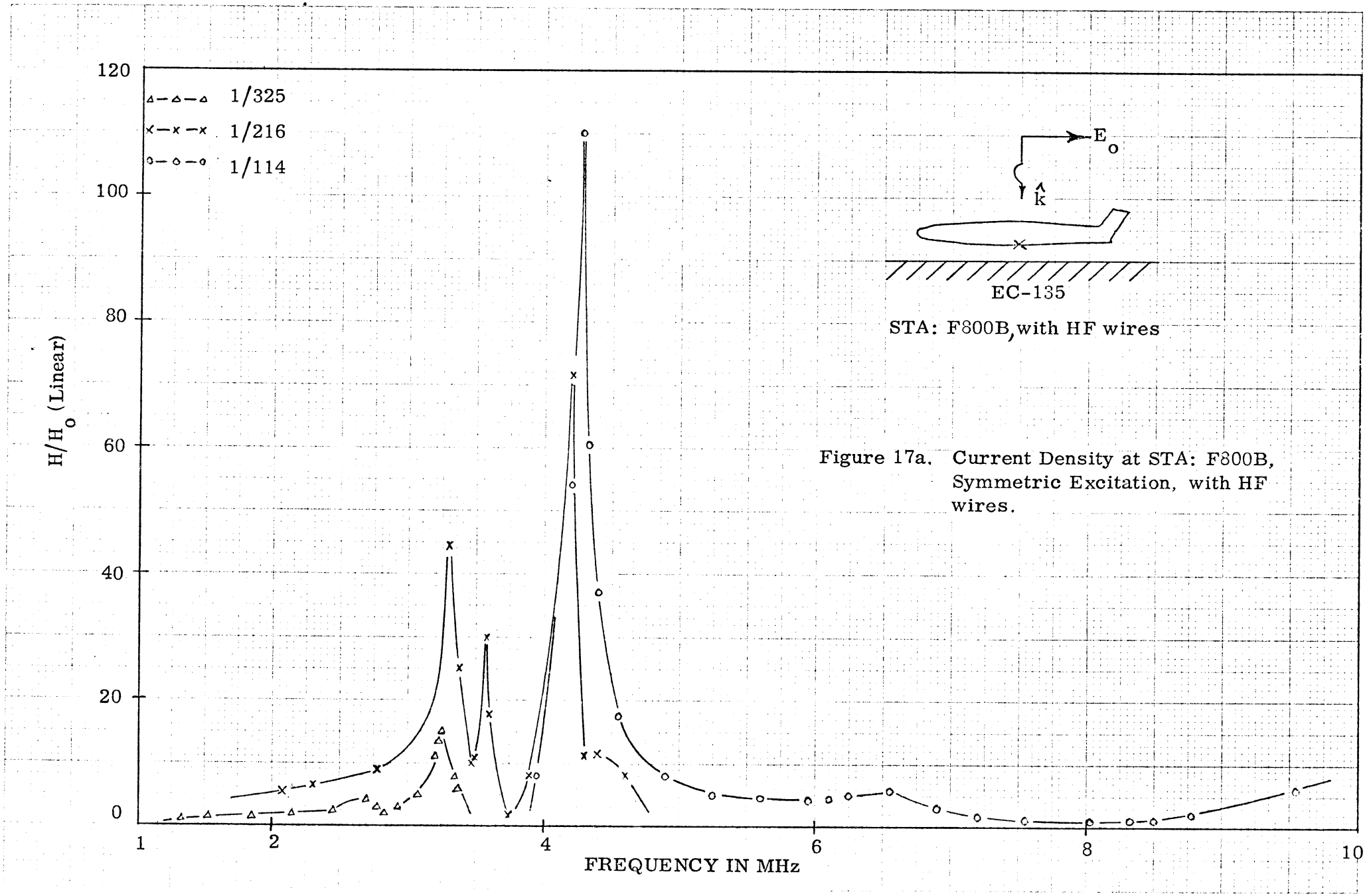

Figure 17a. Current Density at STA: F800B, Symmetric Excitation, with HF wires.

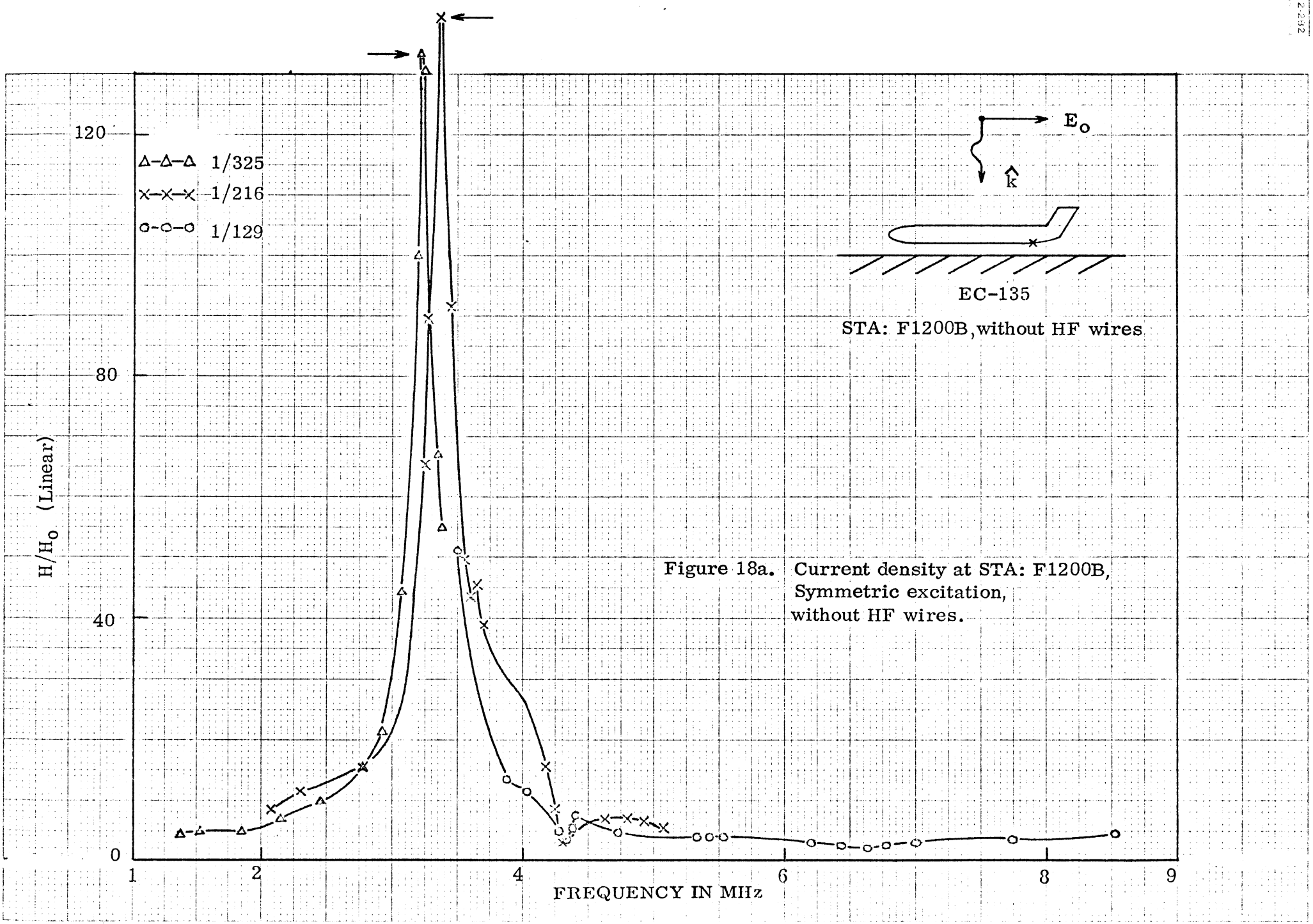

Figure 18a. Current density at STA: F1200B, Symmetric excitation, without HF wires.

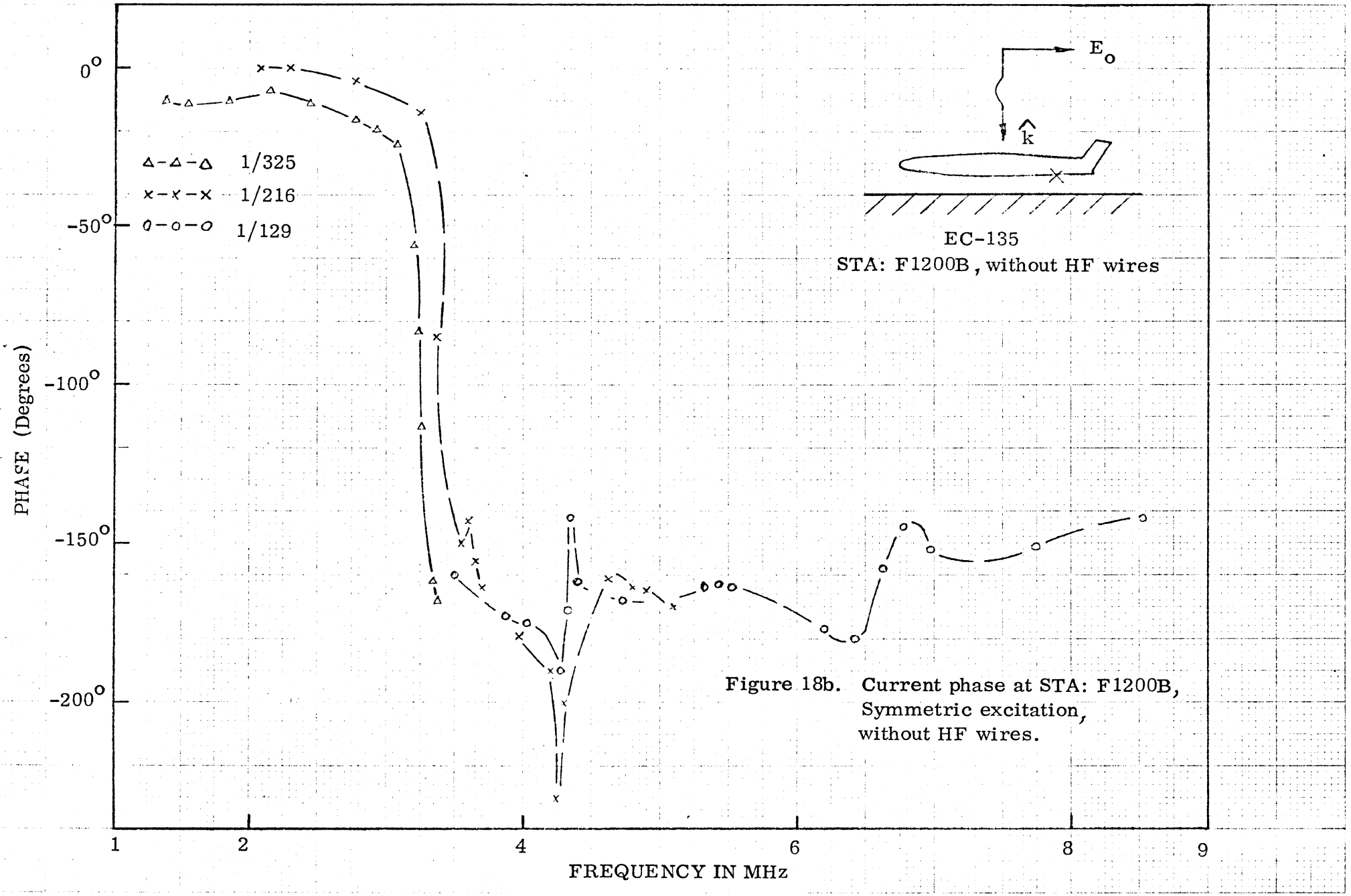

Figure 18b. Current phase at STA: F1200B, Symmetric excitation, without HF wires.

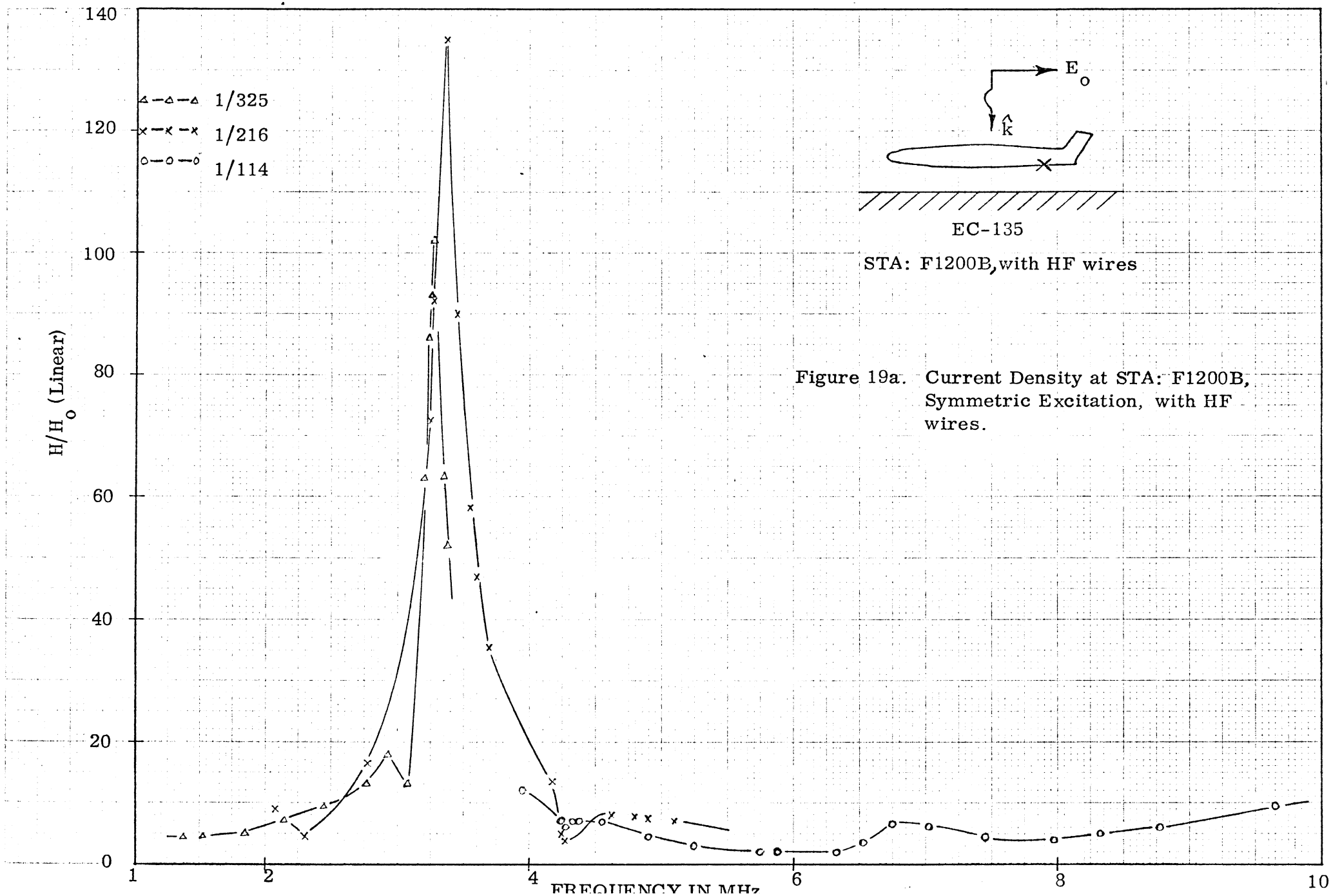

Figure 19a. Current Density at STA: F1200B, Symmetric Excitation, with HF wires.

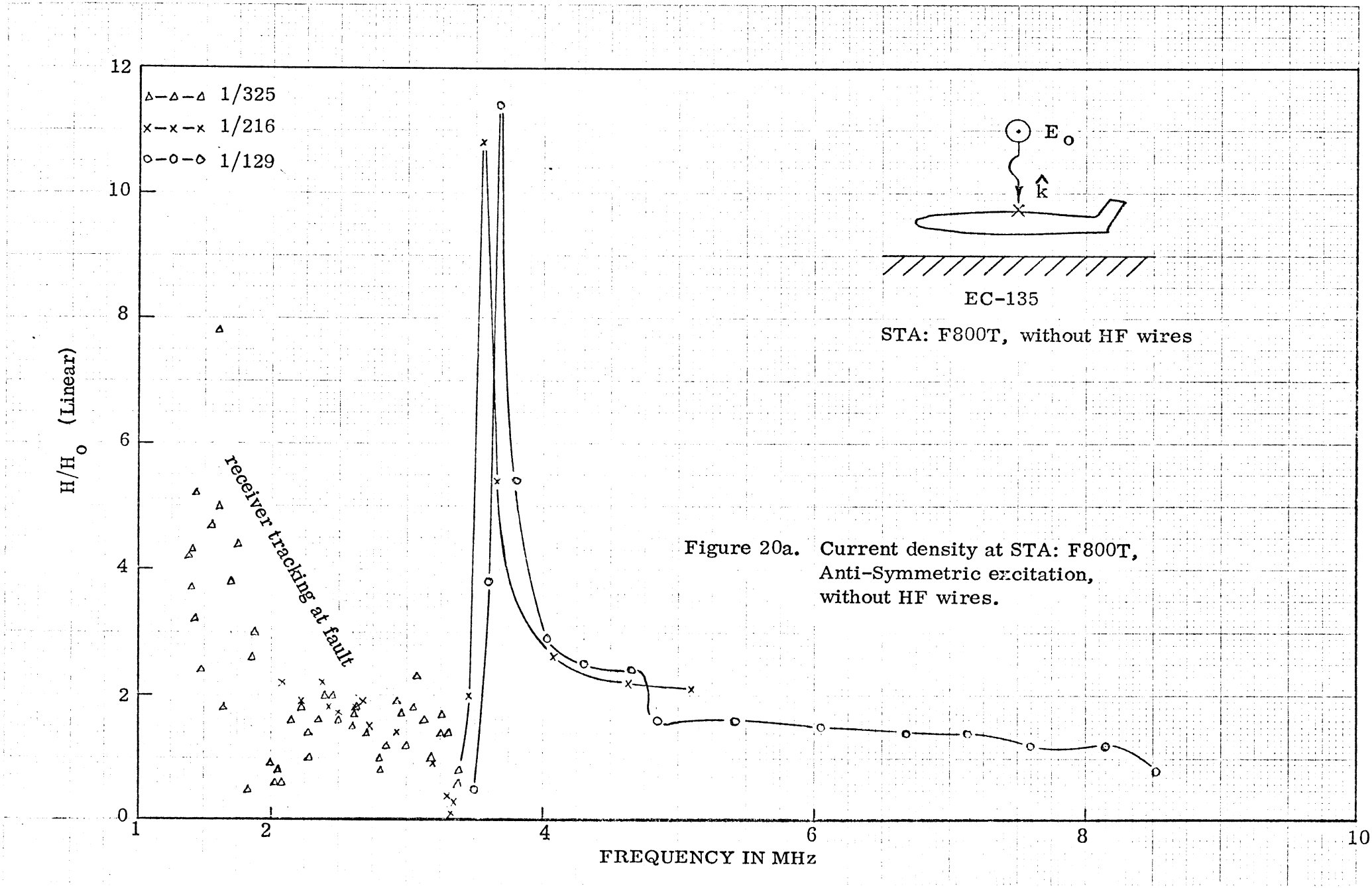

Figure 20a. Current density at STA: F800T, Anti-Symmetric excitation, without HF wires.

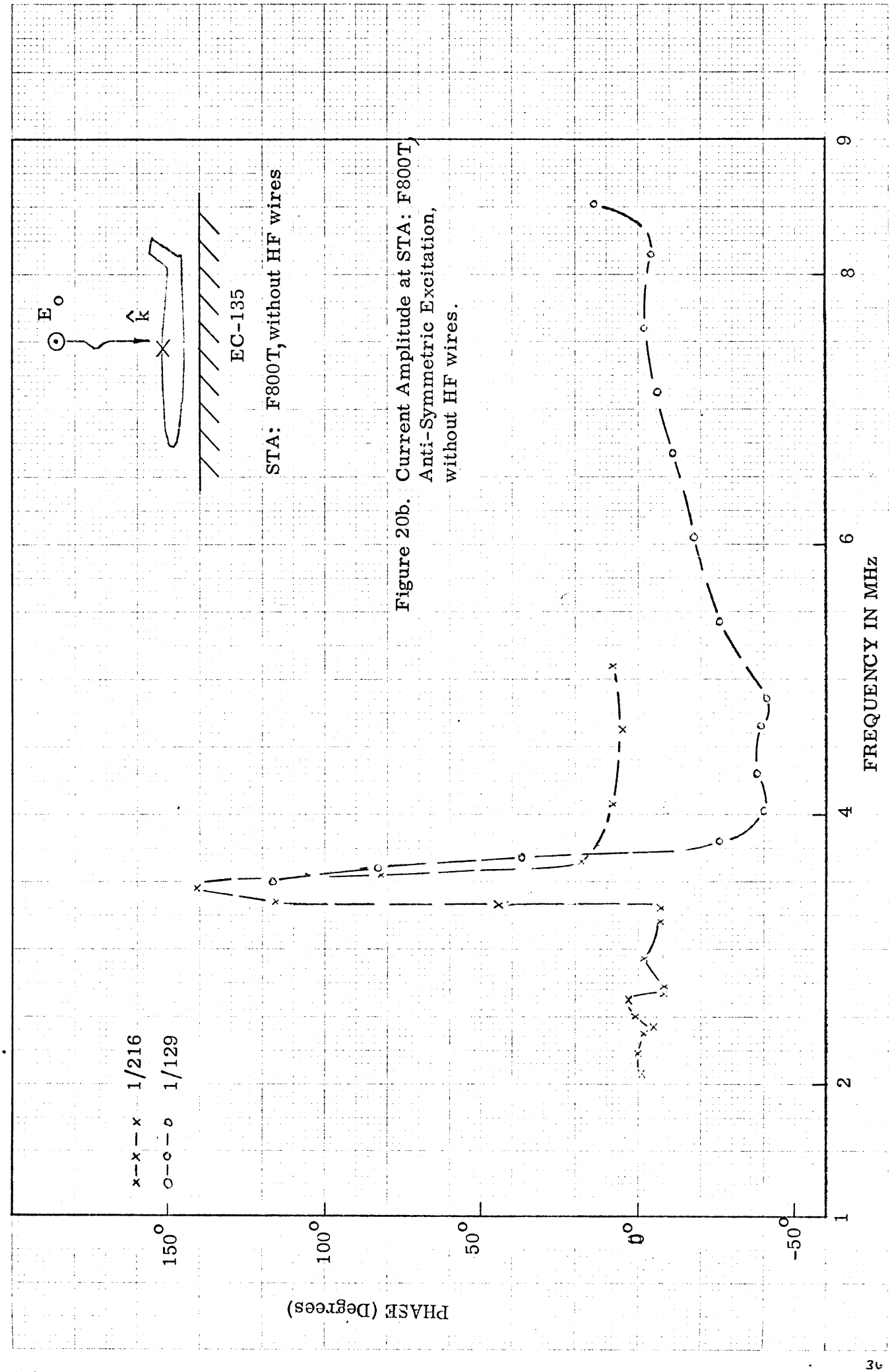

Figure 20b. Current Amplitude at STA: F800T
Anti-Symmetric Excitation,
without HF wires.

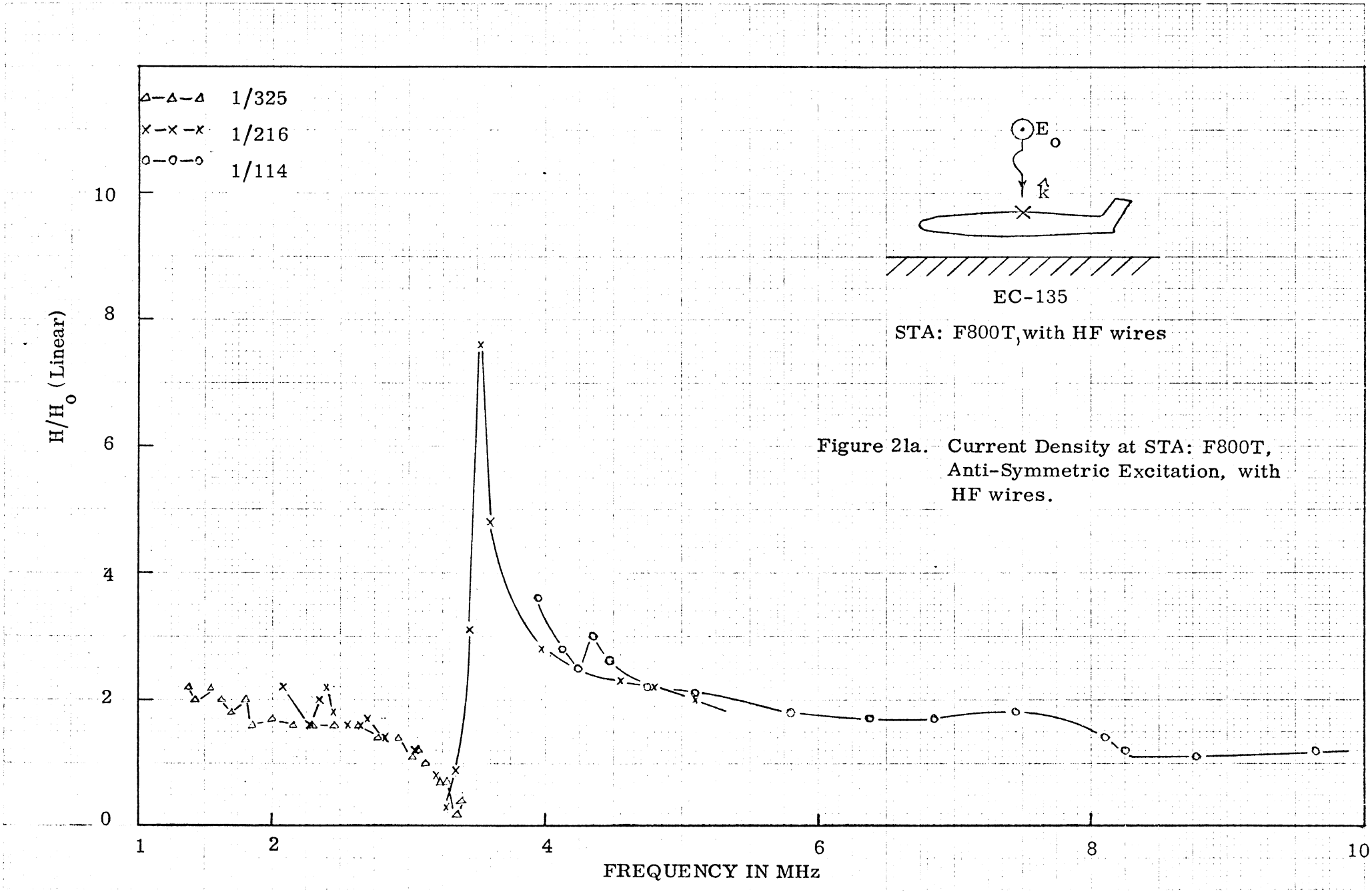

Figure 2la. Current Density at STA: F800T, Anti-Symmetric Excitation, with HF wires.

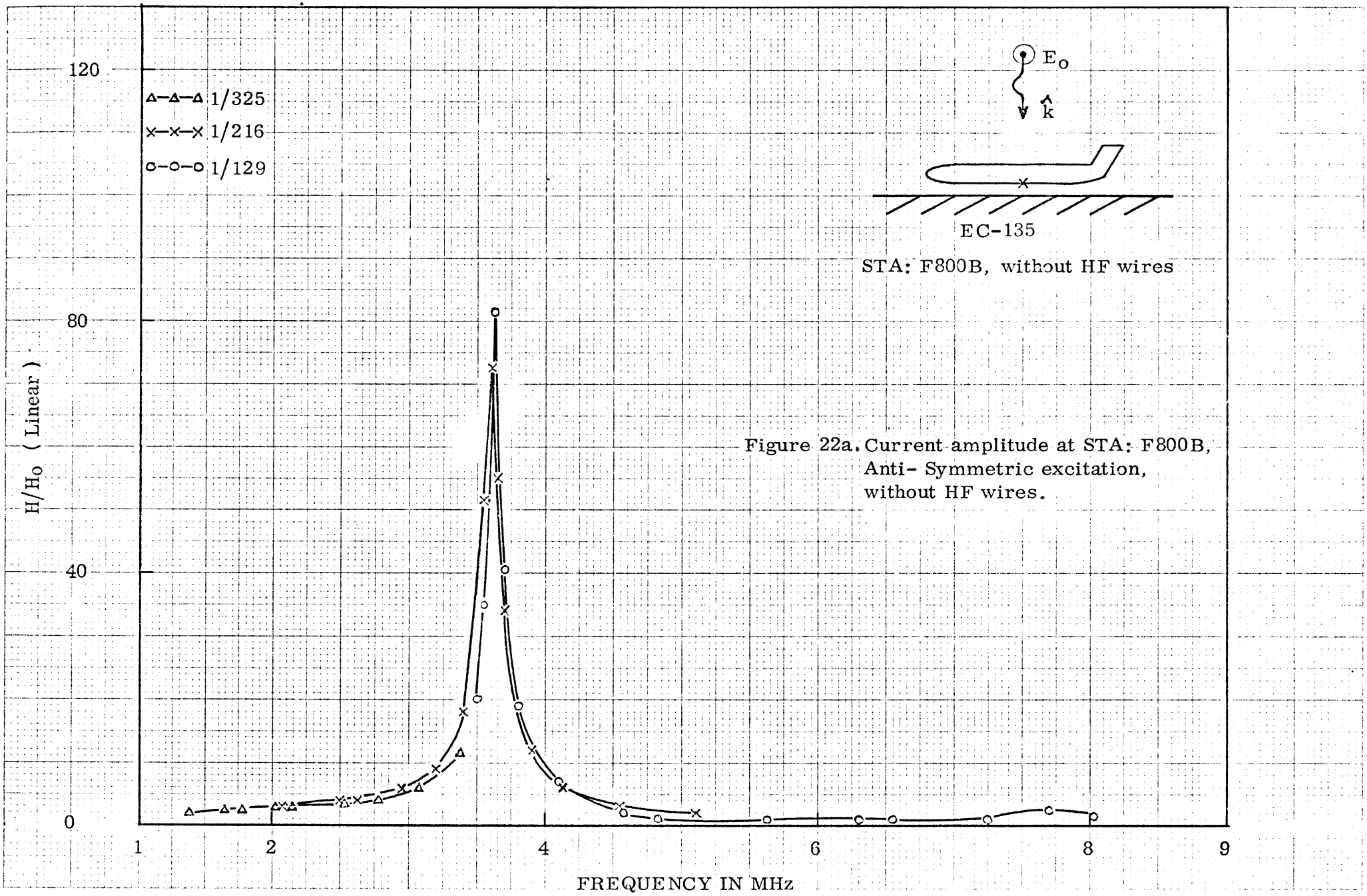

Figure 22a. Current amplitude at STA: F800B, Anti- Symmetric excitation, without HF wires.

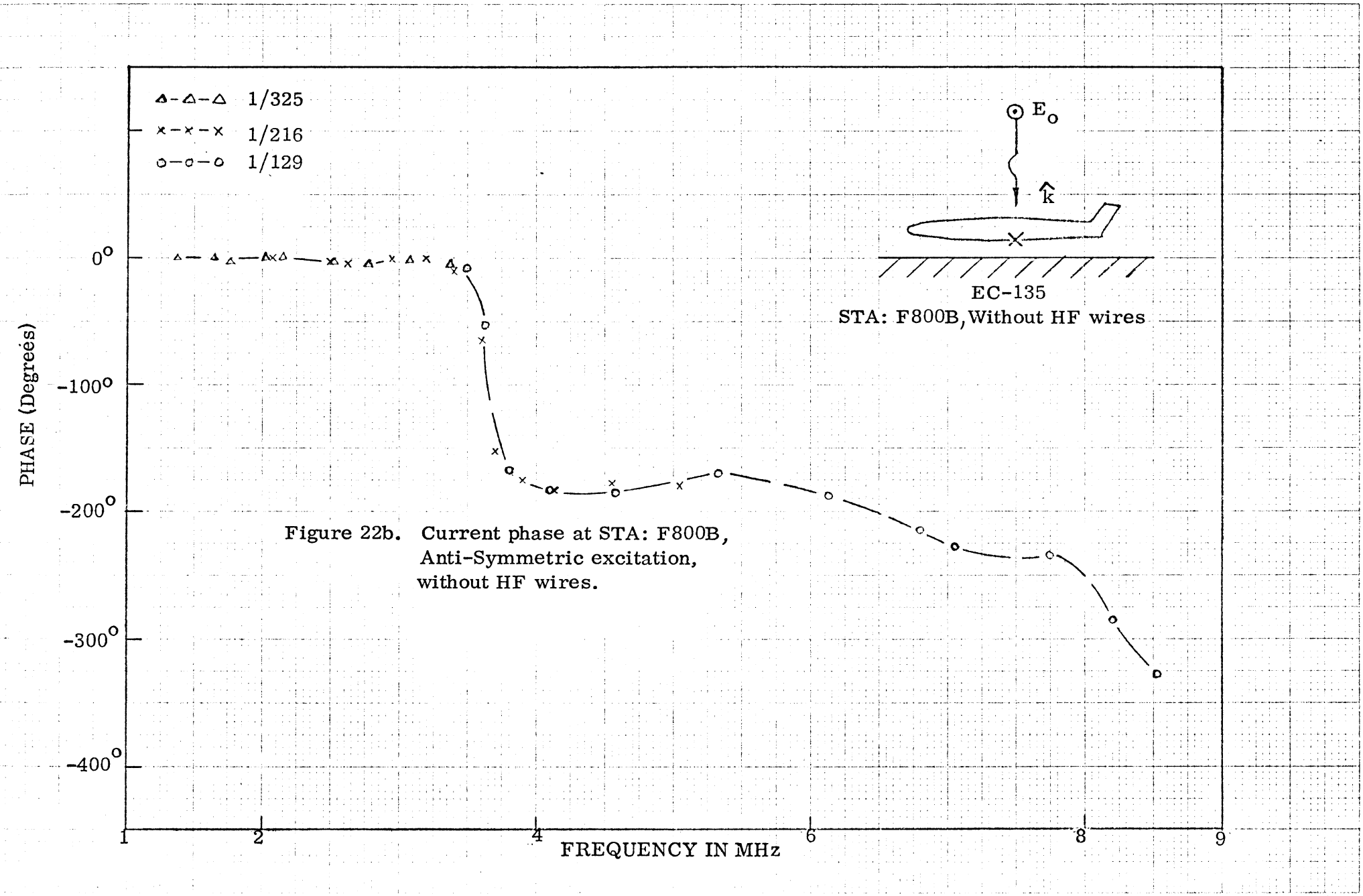

Figure 22b. Current phase at STA: F800B, Anti-Symmetric excitation, without HF wires.

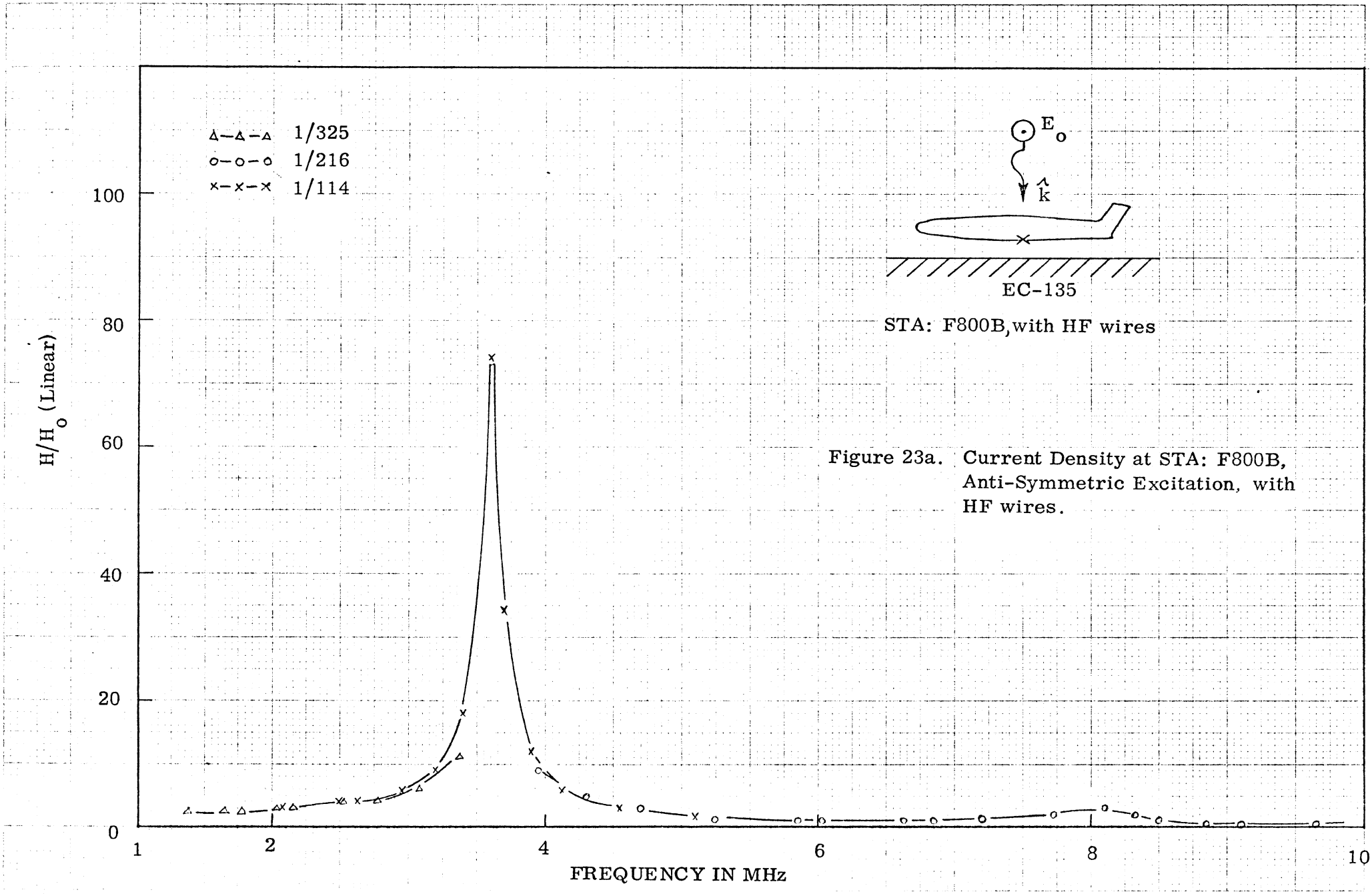

Figure 23a. Current Density at STA: F800B, Anti-Symmetric Excitation, with HF wires.

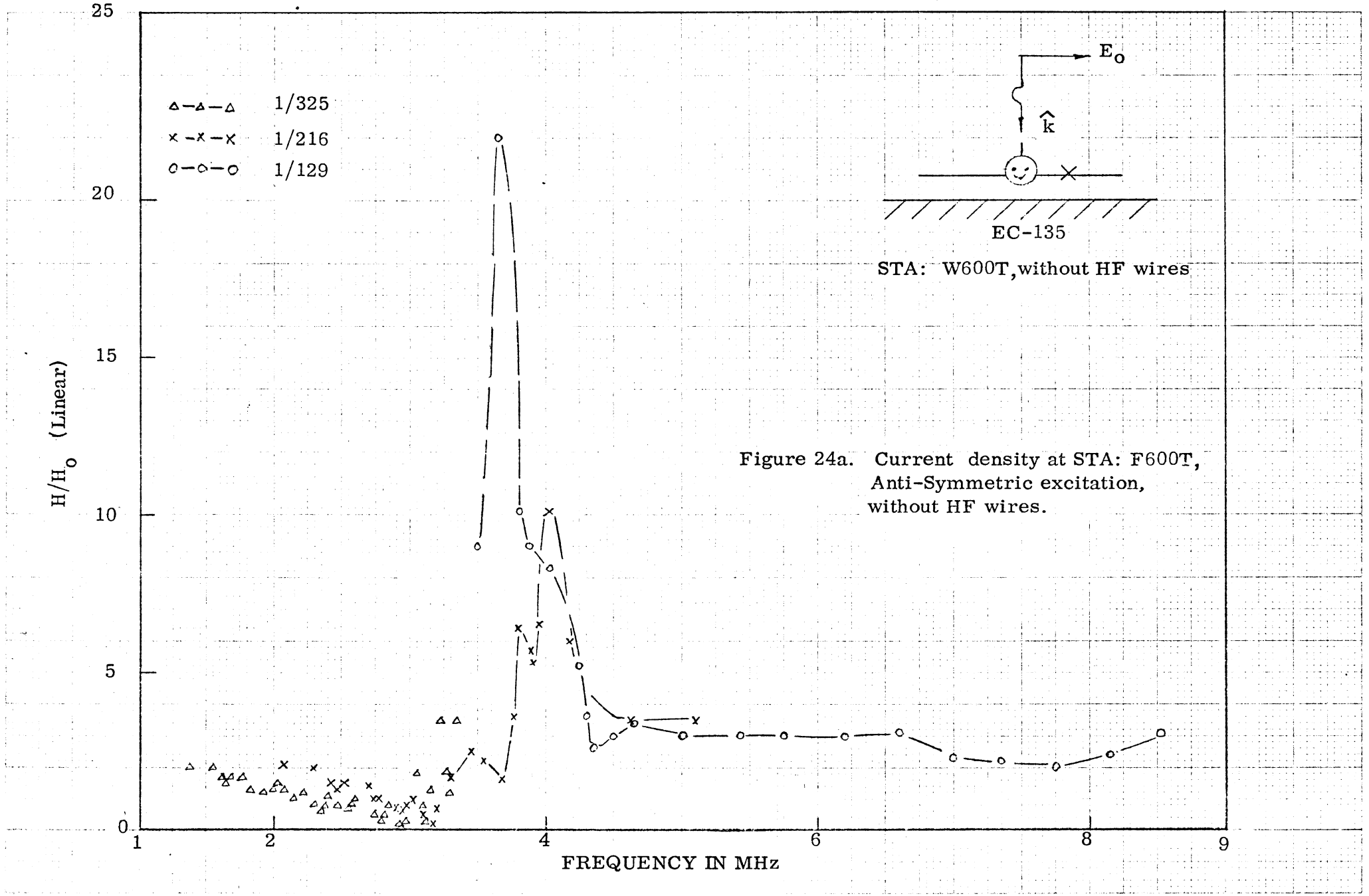

Figure 24a. Current density at STA: F600T, Anti-Symmetric excitation, without HF wires.

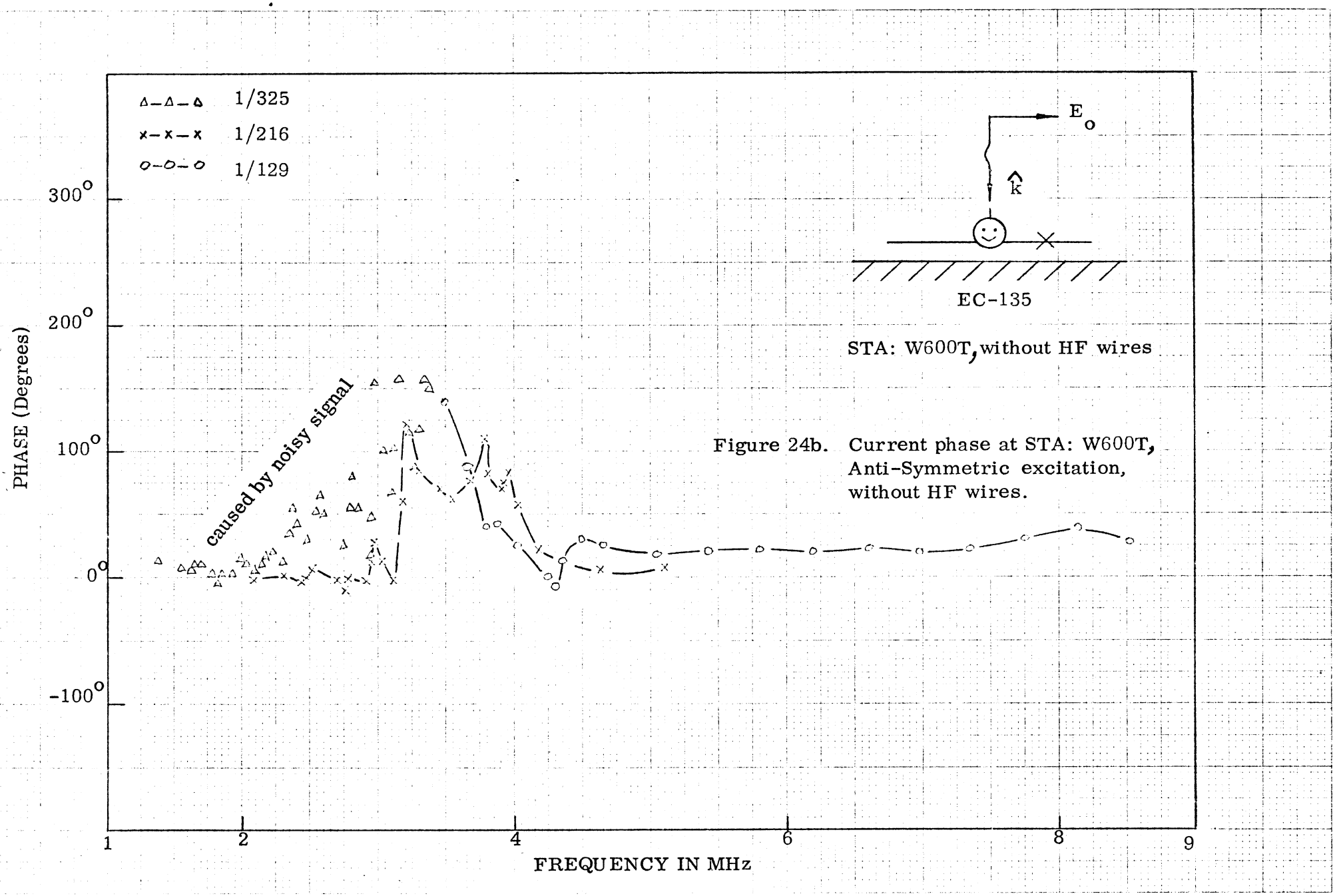

Figure 24b. Current phase at STA: W600T, Anti-Symmetric excitation, without HF wires.

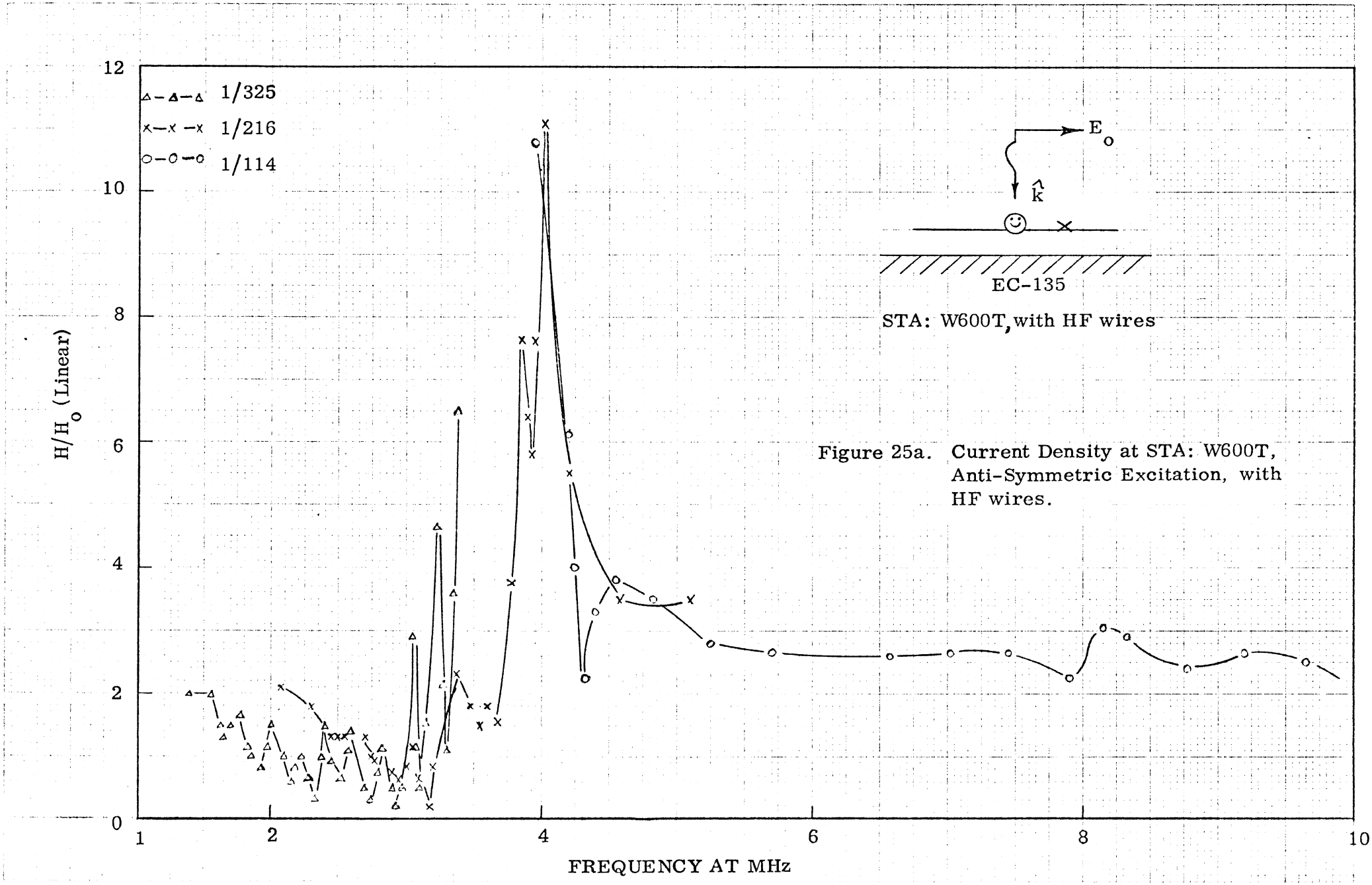

Figure 25a. Current Density at STA: W600T, Anti-Symmetric Excitation, with HF wires.

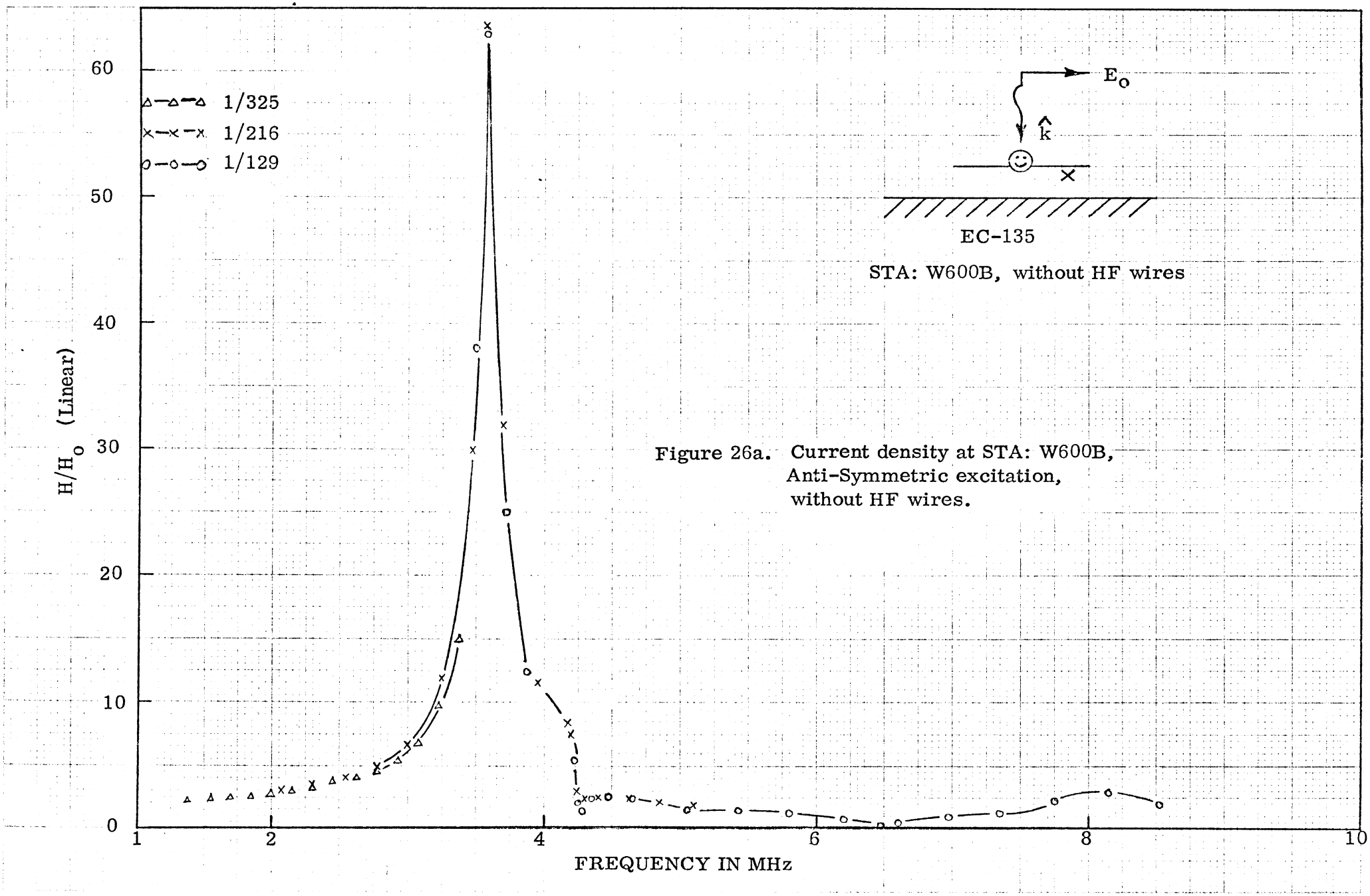

Figure 26a. Current density at STA: W600B, Anti-Symmetric excitation, without HF wires.

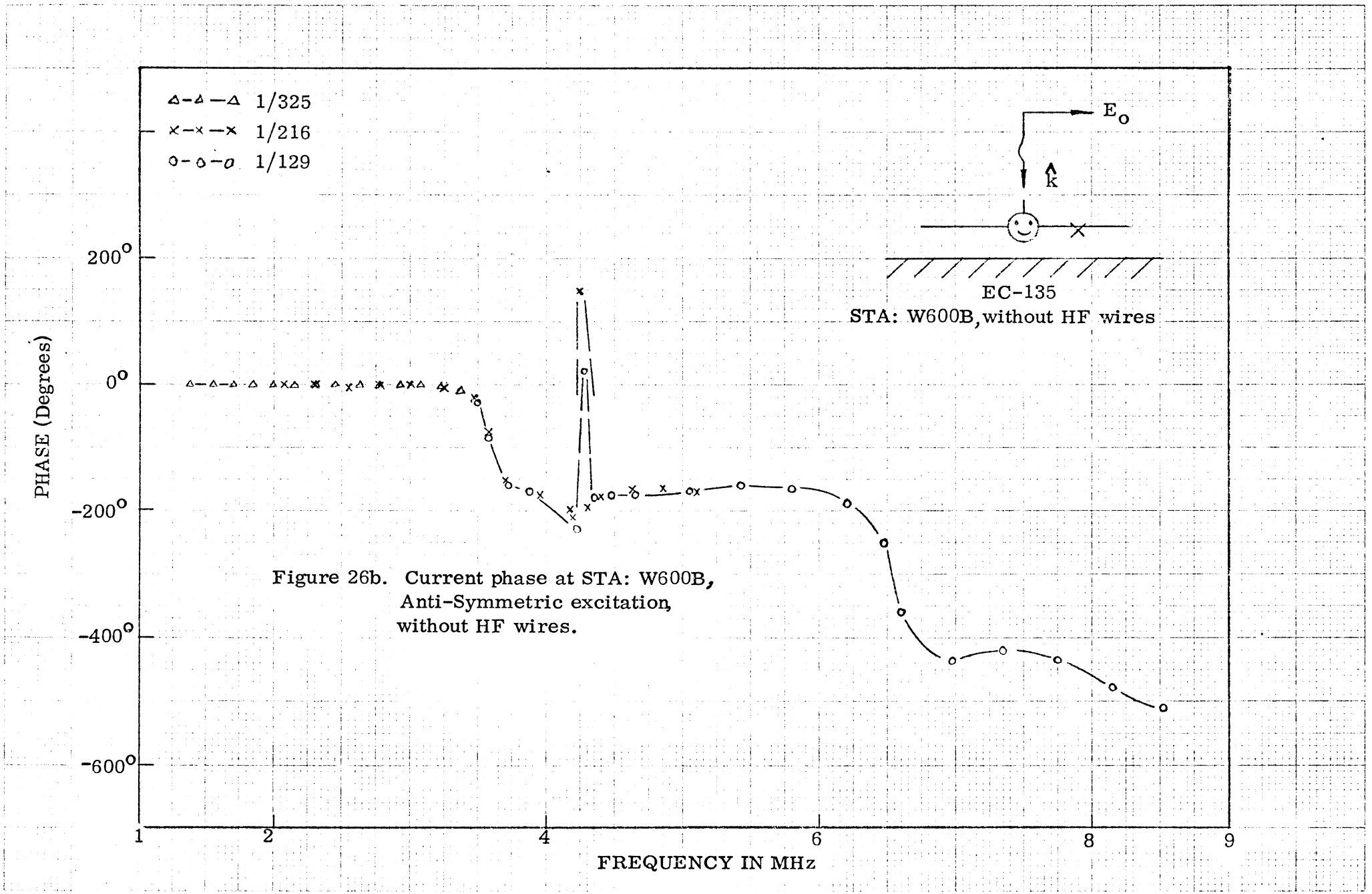

Figure 26b. Current phase at STA: W600B, Anti-Symmetric excitation, without HF wires.

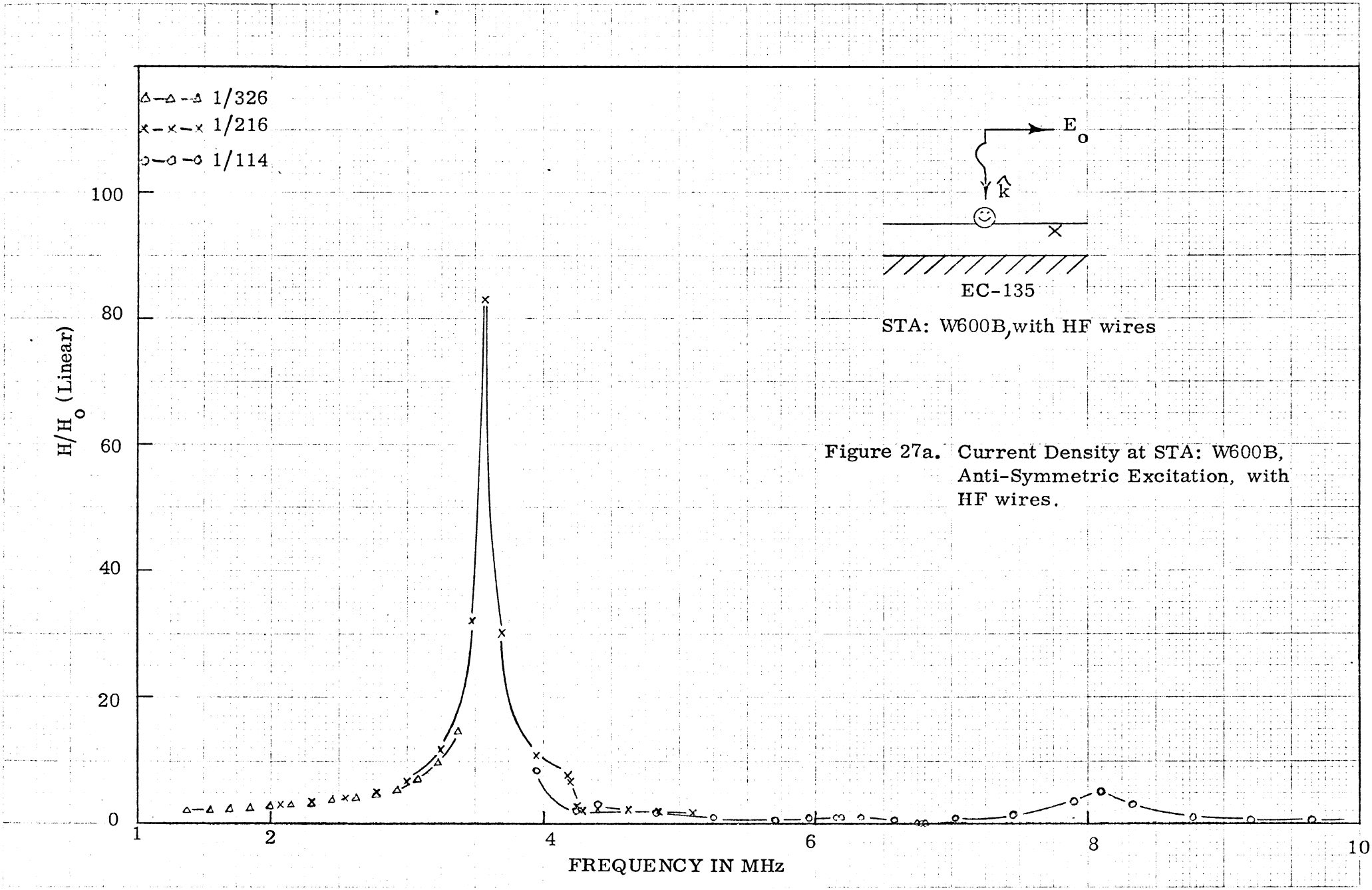

Figure 27a. Current Density at STA: W600B, Anti-Symmetric Excitation, with HF wires.

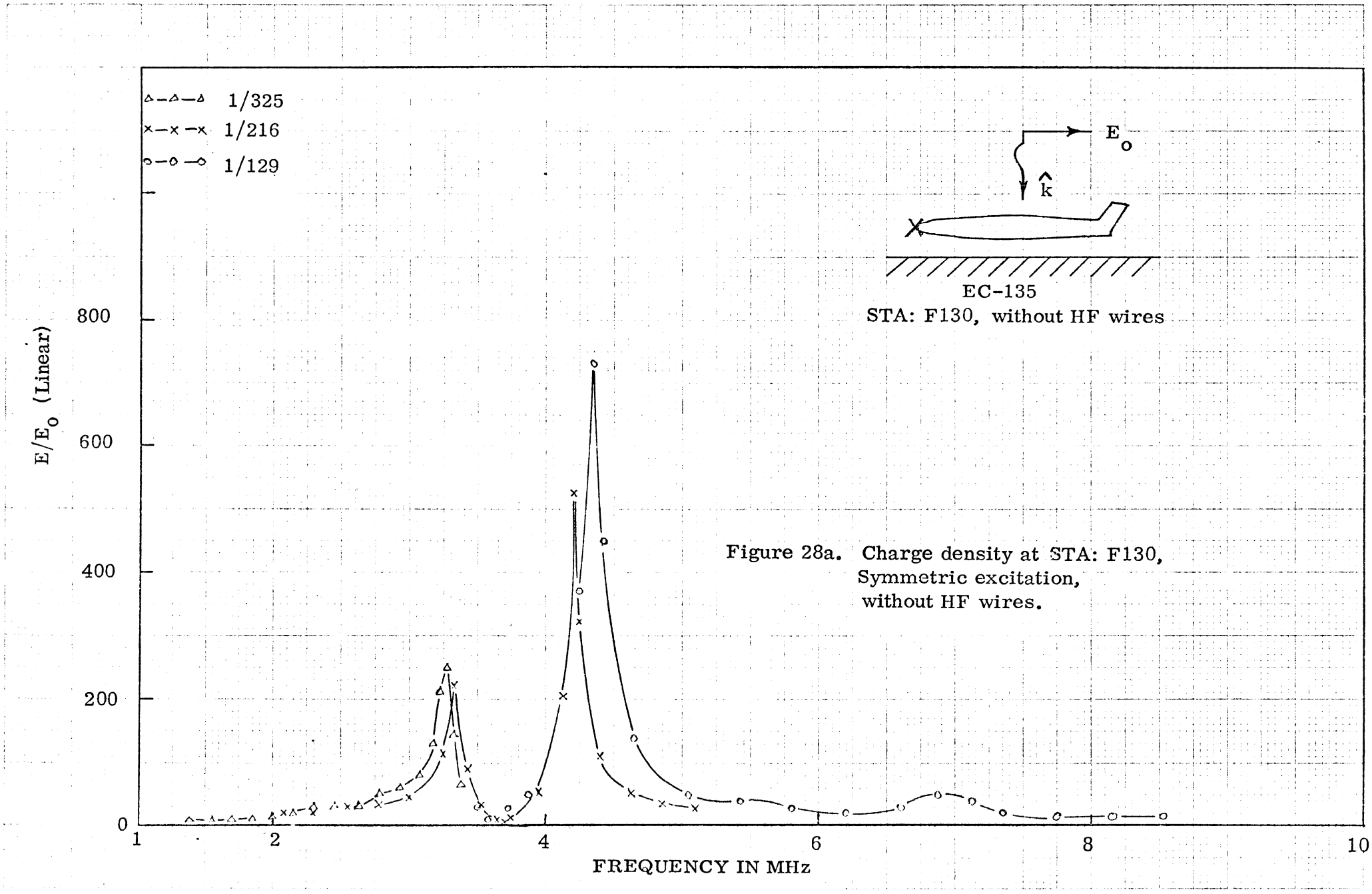

Figure 28a. Charge density at STA: F130, Symmetric excitation, without HF wires.

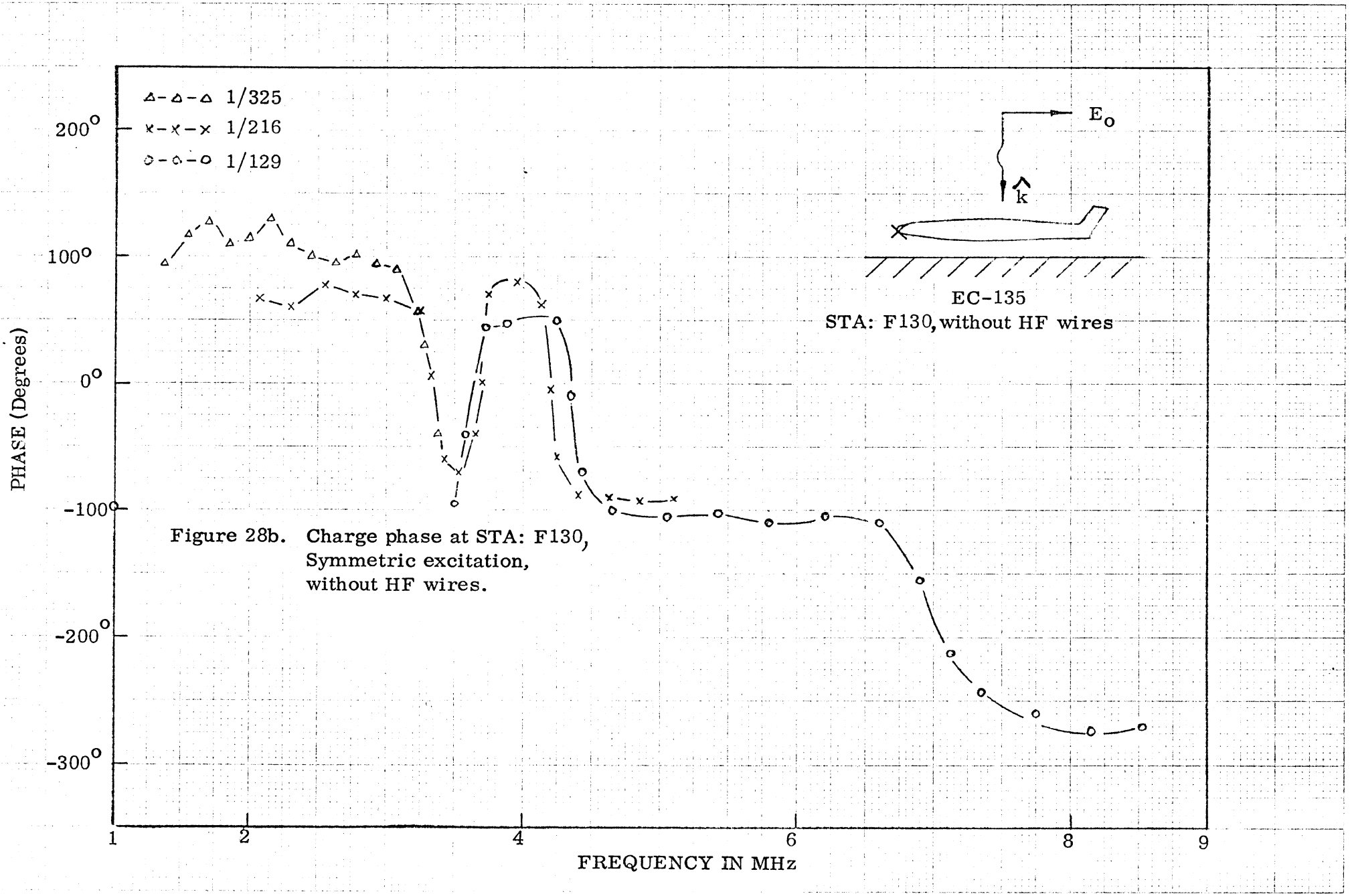

Figure 28b. Charge phase at STA: F130, Symmetric excitation, without HF wires.

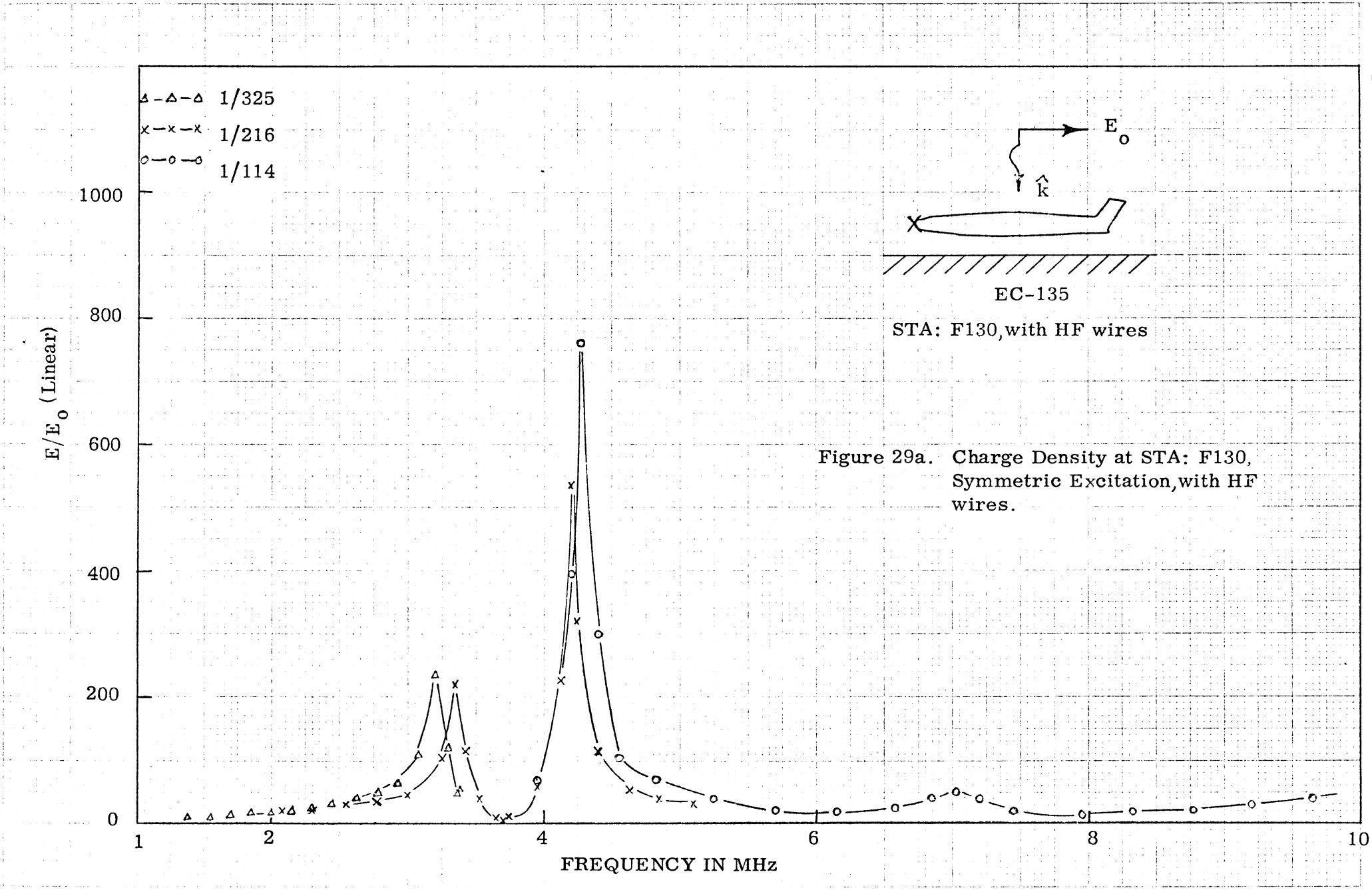

Figure 29a. Charge Density at STA: F130, Symmetric Excitation, with HF wires.

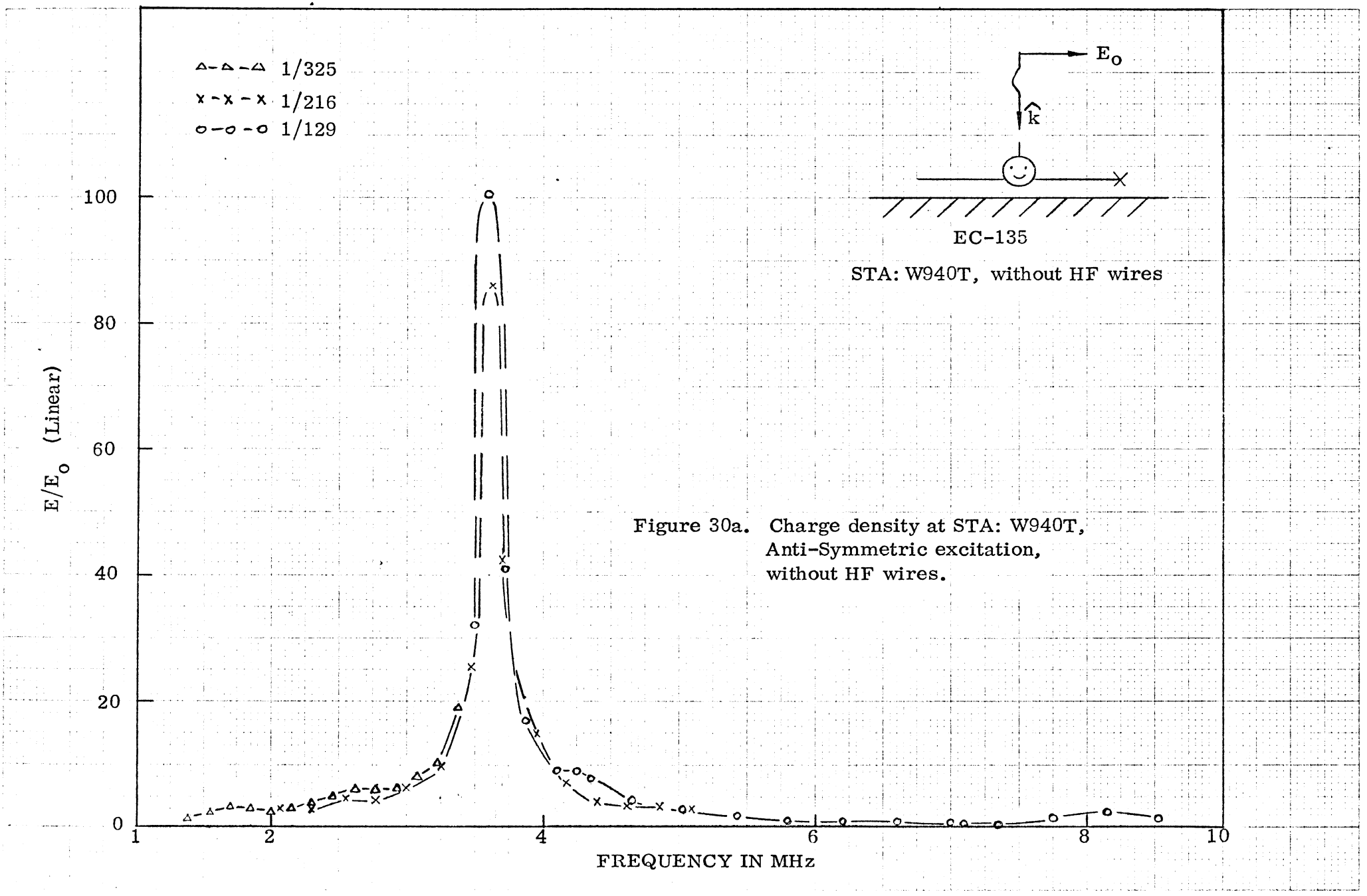

Figure 30a. Charge density at STA: W940T, Anti-Symmetric excitation, without HF wires.

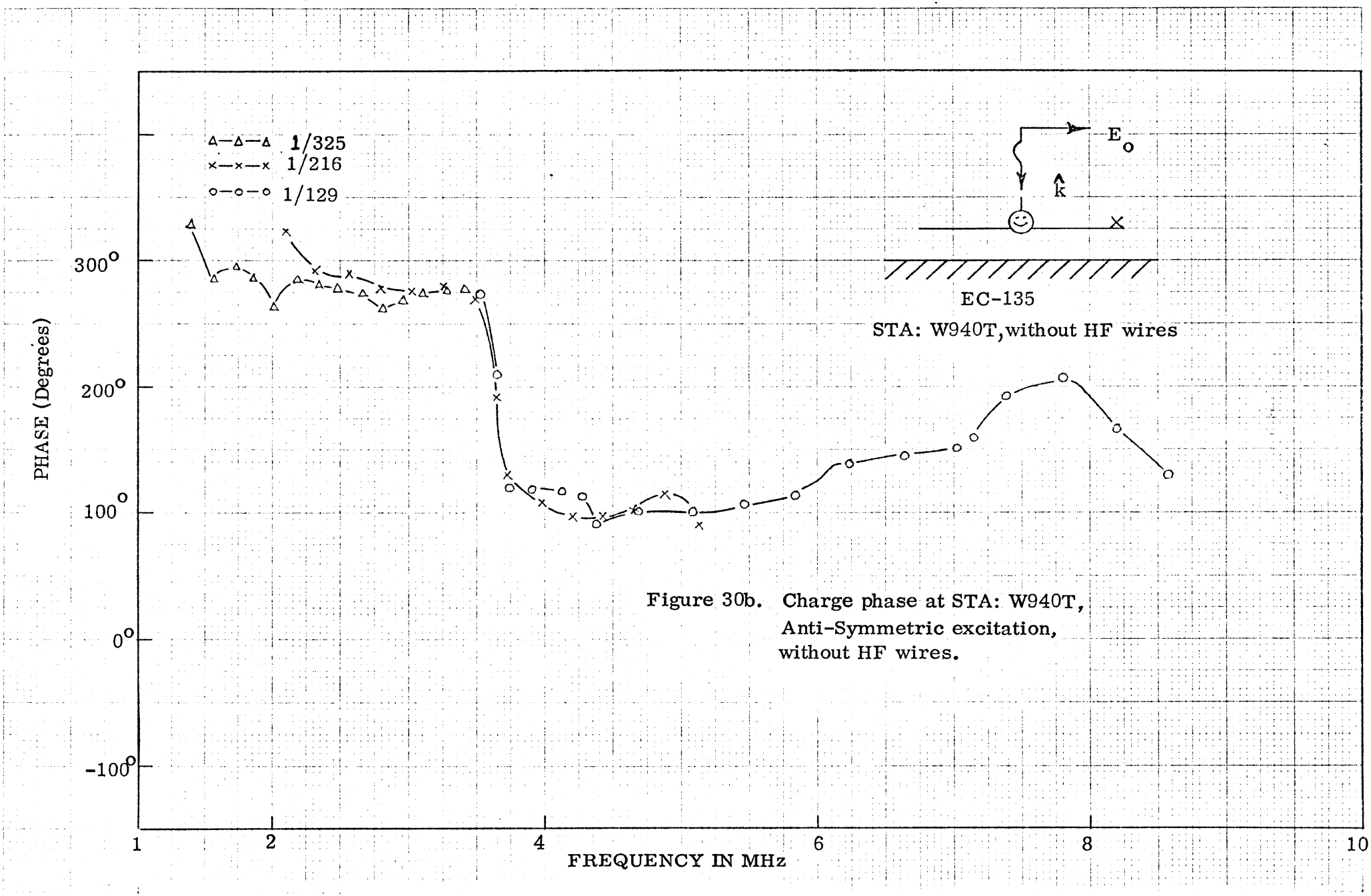

Figure 30b. Charge phase at STA: W940T, Anti-Symmetric excitation, without HF wires.

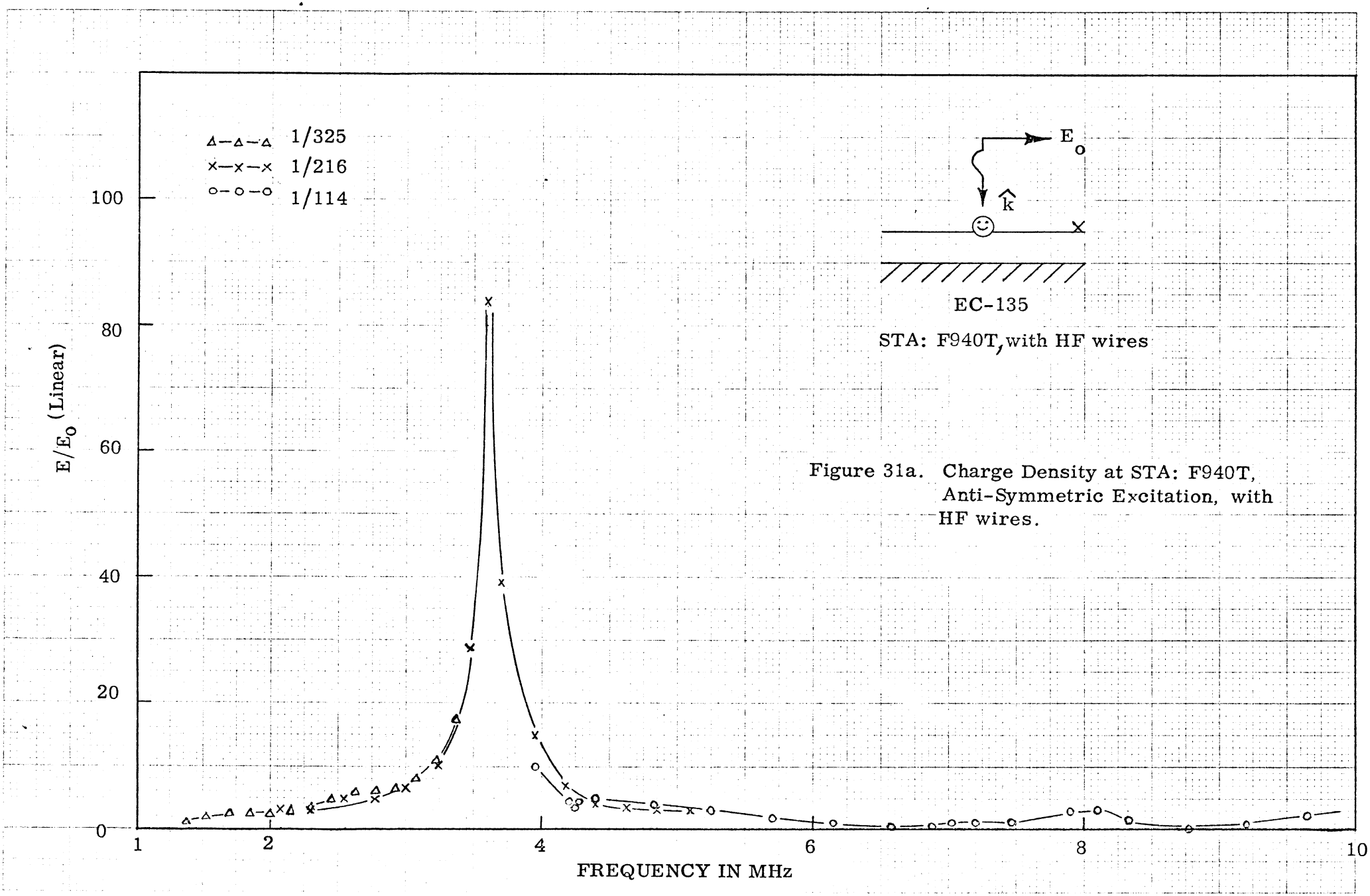

Figure 31a. Charge Density at STA: F940T, Anti-Symmetric Excitation, with HF wires.

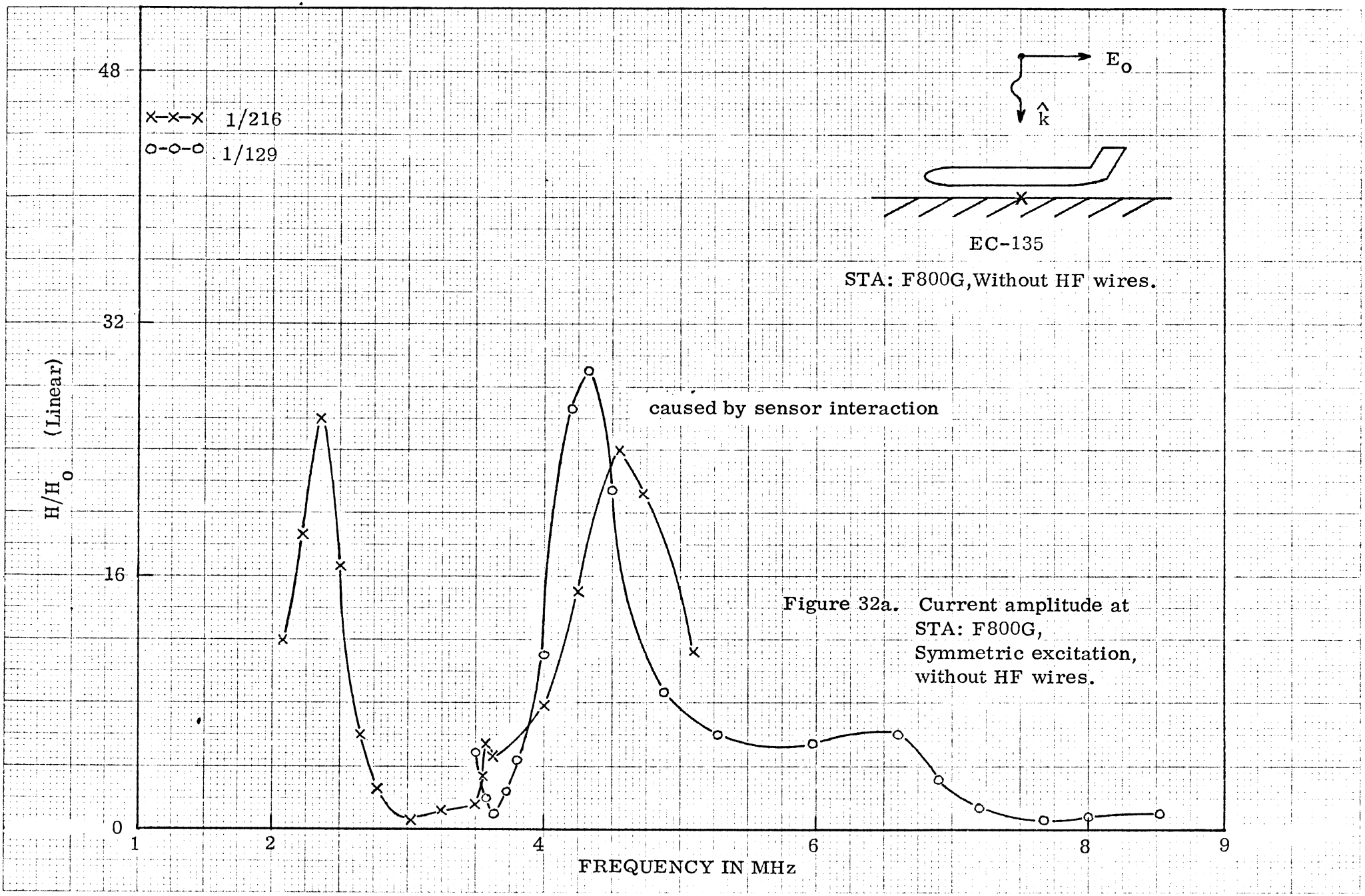

Figure 32a. Current amplitude at STA: F800G, Symmetric excitation, without HF wires.

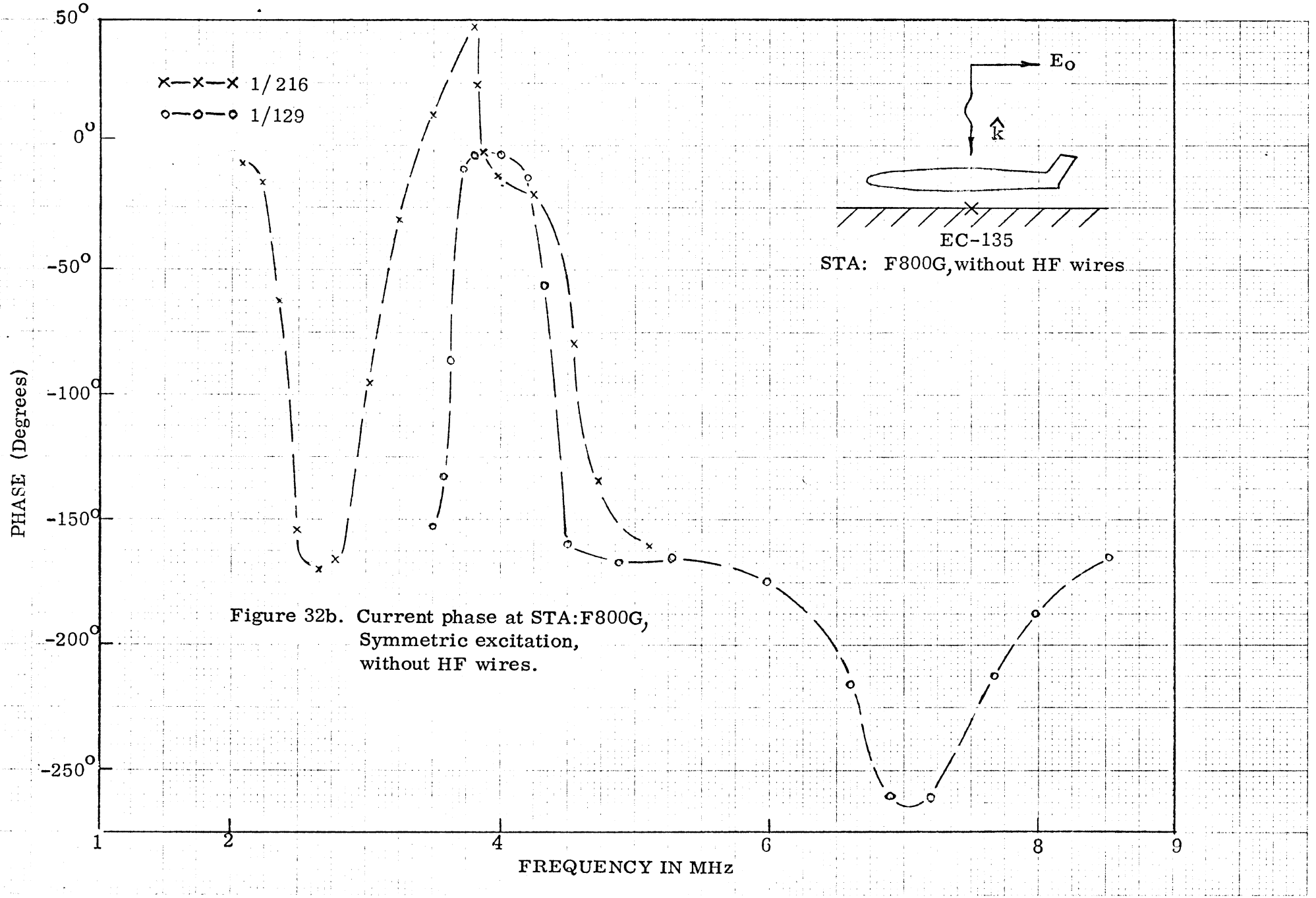

Figure 32b. Current phase at STA:F800G, Symmetric excitation, without HF wires.

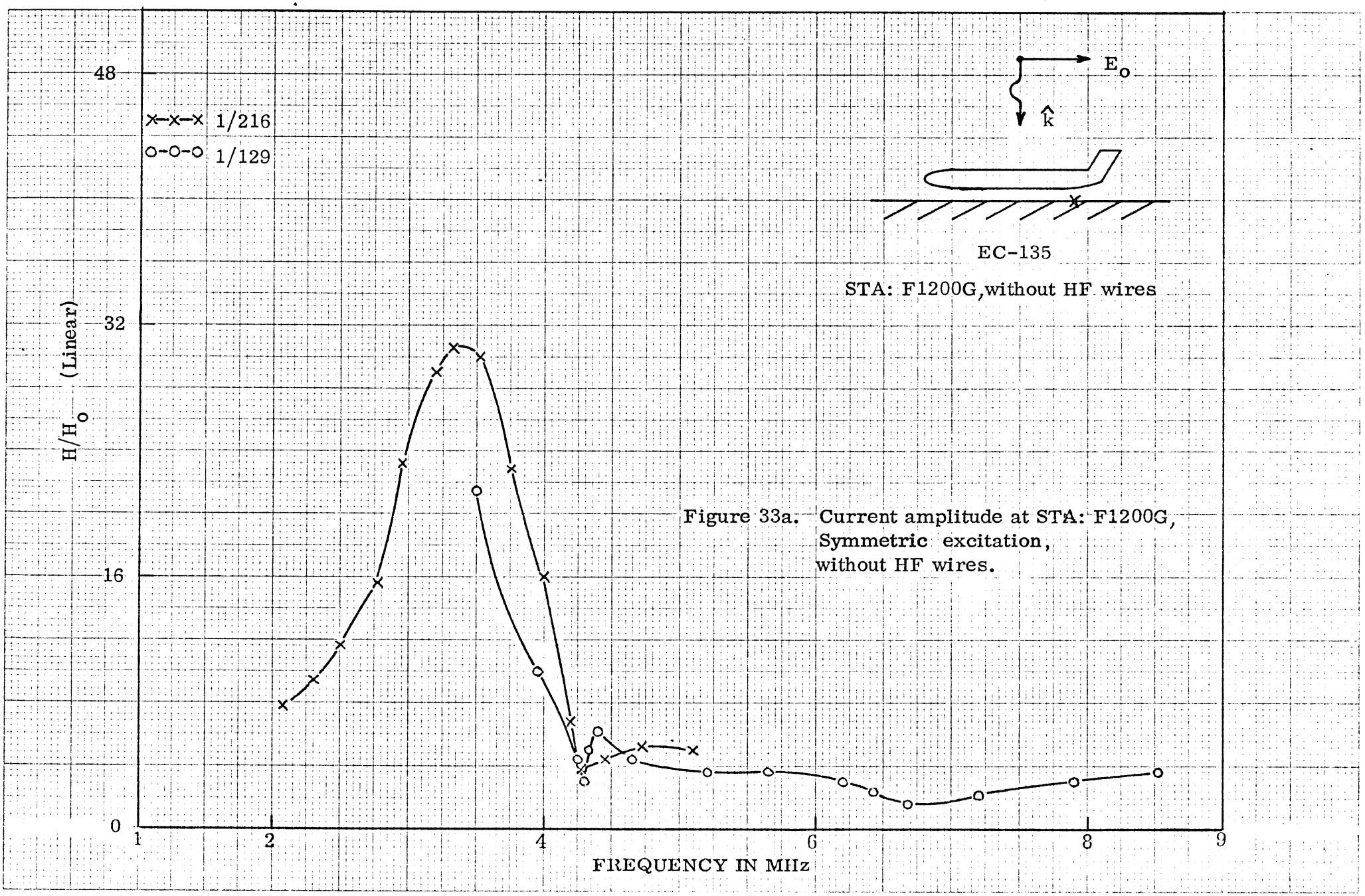

Figure 33a. Current amplitude at STA: F1200G, Symmetric excitation, without HF wires.

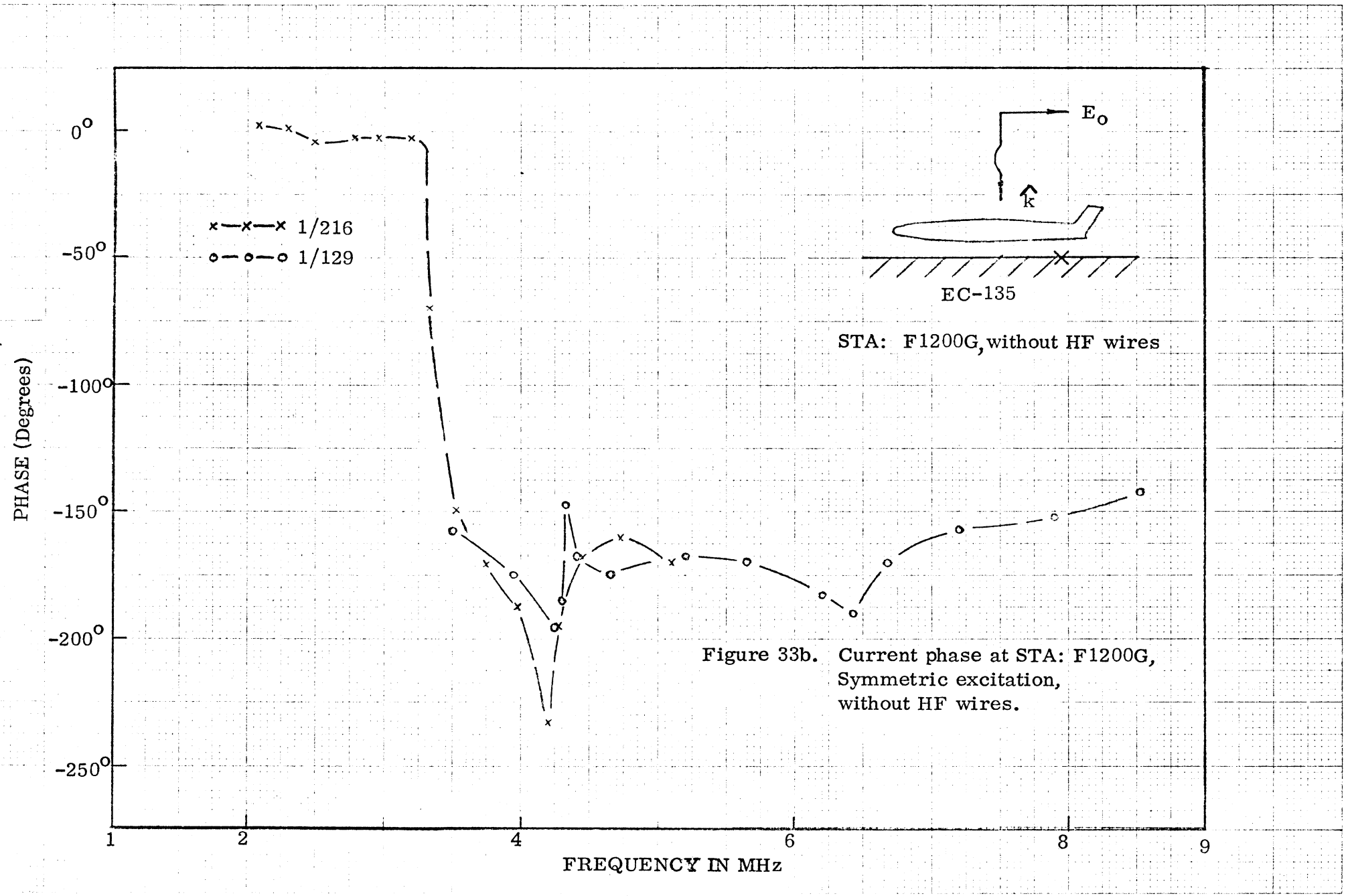

Figure 33b. Current phase at STA: F1200G, Symmetric excitation, without HF wires.

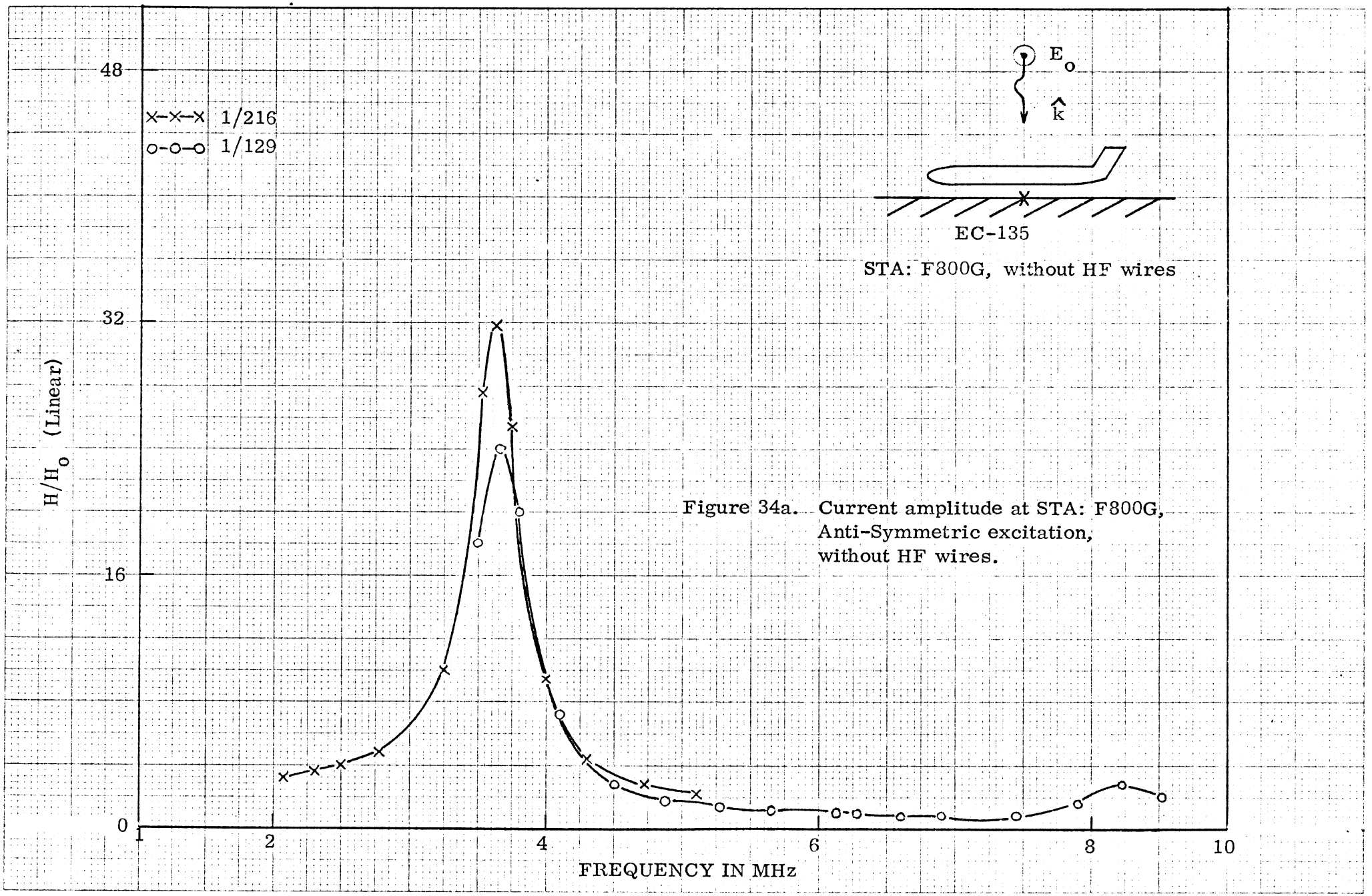

Figure 34a. Current amplitude at STA: F800G, Anti-Symmetric excitation, without HF wires.

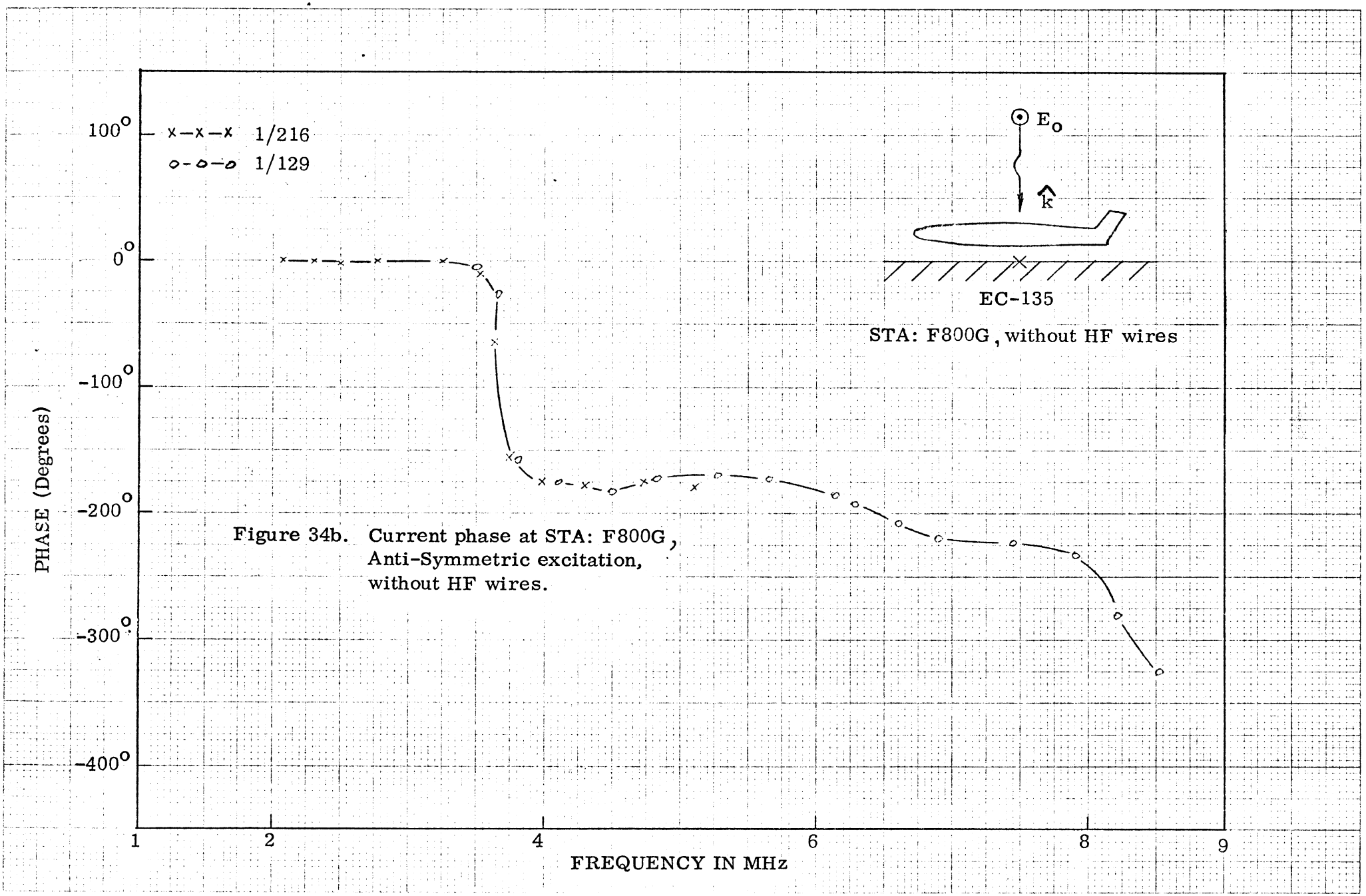

Figure 34b. Current phase at STA: F800G, Anti-Symmetric excitation, without HF wires.

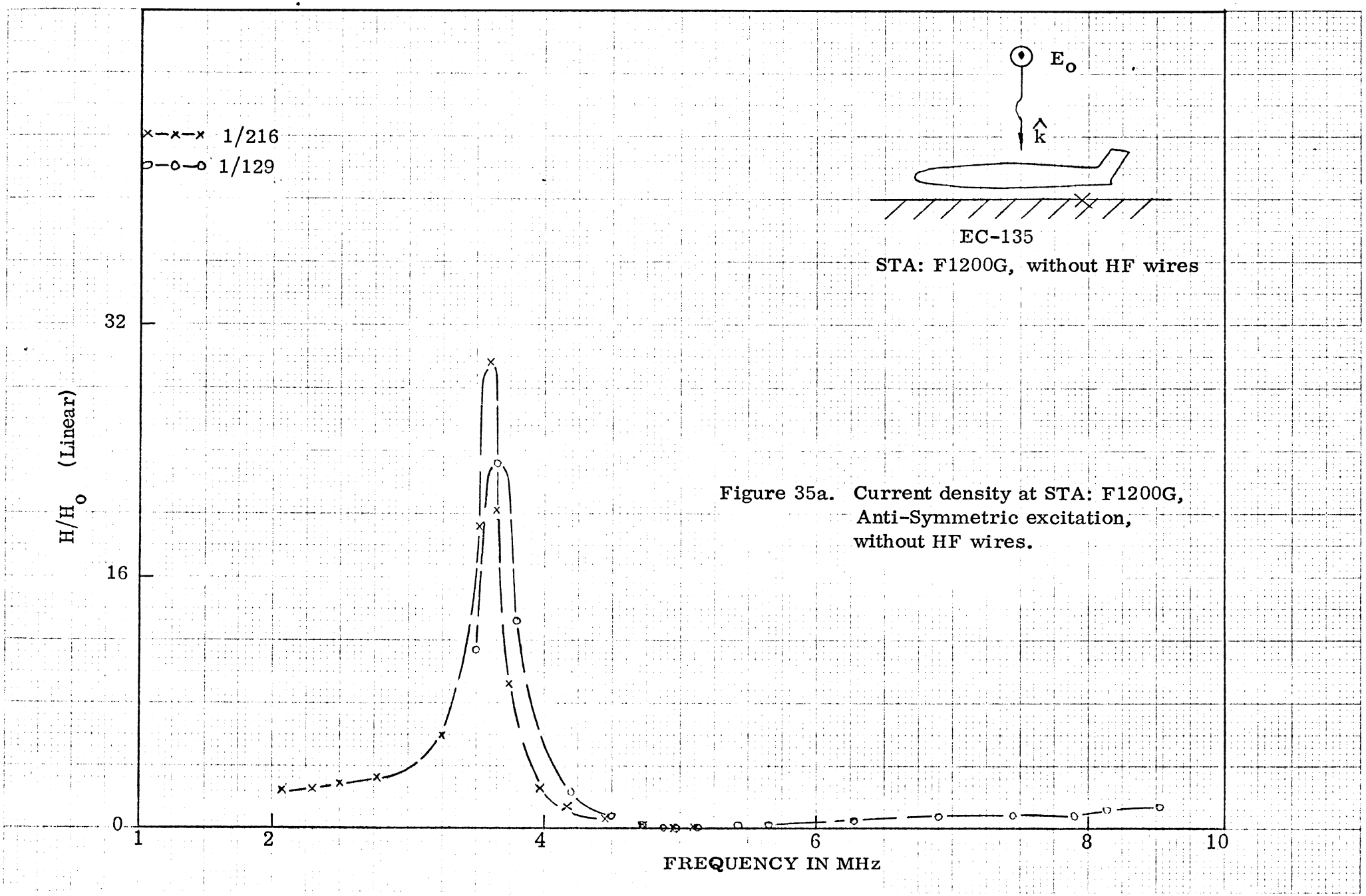

Figure 35a. Current density at STA: F1200G, Anti-Symmetric excitation, without HF wires.

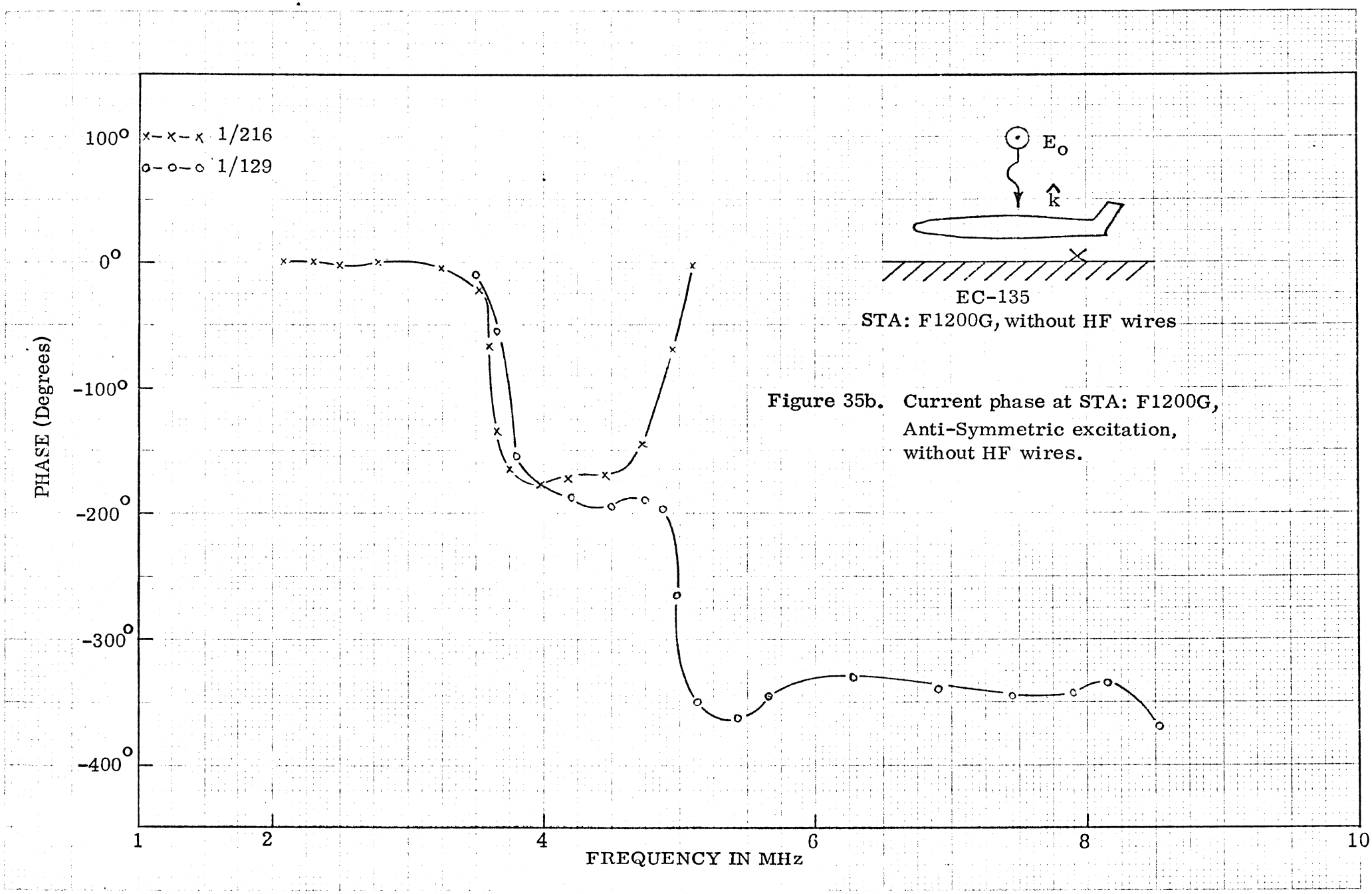

Figure 35b. Current phase at STA: F1200G, Anti-Symmetric excitation, without HF wires.